

Winter 2010

# Linearity tests of a multibeam echosounder

Samuel F. Greenaway  
*University of New Hampshire, Durham*

Follow this and additional works at: <https://scholars.unh.edu/thesis>

---

## Recommended Citation

Greenaway, Samuel F., "Linearity tests of a multibeam echosounder" (2010). *Master's Theses and Capstones*. 596.  
<https://scholars.unh.edu/thesis/596>

This Thesis is brought to you for free and open access by the Student Scholarship at University of New Hampshire Scholars' Repository. It has been accepted for inclusion in Master's Theses and Capstones by an authorized administrator of University of New Hampshire Scholars' Repository. For more information, please contact [nicole.hentz@unh.edu](mailto:nicole.hentz@unh.edu).

LINEARITY TESTS OF A MULTIBEAM ECHOSOUNDER

BY

SAMUEL F. GREENAWAY  
Sc B. Physics, Brown University, 1998

THESIS

Submitted to the University of New Hampshire  
in Partial Fulfillment of  
the Requirements for the Degree of

Master of Science  
in  
Ocean Engineering

December, 2010

UMI Number: 1489946

All rights reserved

**INFORMATION TO ALL USERS**

The quality of this reproduction is dependent upon the quality of the copy submitted.

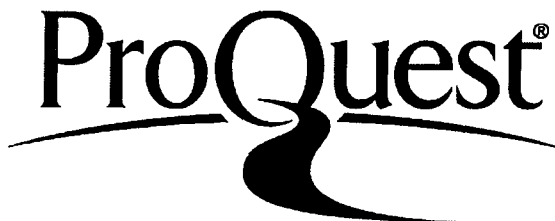
In the unlikely event that the author did not send a complete manuscript and there are missing pages, these will be noted. Also, if material had to be removed, a note will indicate the deletion.



UMI 1489946

Copyright 2011 by ProQuest LLC.

All rights reserved. This edition of the work is protected against unauthorized copying under Title 17, United States Code.



ProQuest LLC  
789 East Eisenhower Parkway  
P.O. Box 1346  
Ann Arbor, MI 48106-1346

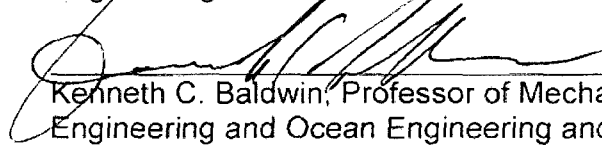
This thesis has been examined and approved.



\_\_\_\_\_  
Thesis Director, Thomas C. Weber, Research  
Assistant Professor of Marine Sciences and Ocean  
Engineering



\_\_\_\_\_  
Andrew Armstrong, Affiliate Professor of Ocean  
Engineering and Marine Sciences and Earth Sciences



\_\_\_\_\_  
Kenneth C. Baldwin, Professor of Mechanical  
Engineering and Ocean Engineering and Marine  
Sciences

02 Dec 2010

Date

## TABLE OF CONTENTS

LIST OF TABLES.....	iv
LIST OF FIGURES.....	v
ABSTRACT.....	vii
CHAPTER	PAGE
INTRODUCTION.....	1
1. TANK TESTING OF A MULTIBEAM ECHOSOUNDER.....	6
Description of the 7125 System.....	7
Test Tank Acquisition.....	8
Test Tank Configuration.....	8
Linearity of Element Response with Respect to Power and Gain Settings.....	10
Tank Hydrophone Linearity Results.....	14
Model Fit.....	18
Measure of Non-Linearity, 1dB Compression Points.....	23
Discussion.....	27
Linearity of Beam Formed Response with Respect to power and Gain Settings.....	29
Discussion.....	34
Prediction of Returned SPL and the APL-UW Model.....	35
Discussion.....	39
2. FIED TESTING OF A MULTIBEAM ECHOSOUNDER.....	41
Field Acquisition Discussion.....	50
3. EFFECT OF NON-LINEARITY ON BACKSCATTER AND BATHYMETRY.....	54
Effect of Non-Linearity on Backscatter.....	56
Effect of non-Linearity on Beam Forming and Bathymetric Detection.....	61
4. CONCLUSION.....	67
REFERENCES.....	69

## LIST OF TABLES

Table 1: Field Linearity Measurements.....	42
--	----

## LIST OF FIGURES

Figure 1: Assumed electronic schematic of sonar receiver .....	8
Figure 2: Calibration Tank Facility (from Lanzoni <i>et al.</i> , 2009).....	9
Figure 3: Hydrophone element output. One trace is from center element of array. The other is from element at end of array. The data selected for analysis is indicated by the box.....	12
Figure 4: 200 kHz hydrophone output as a function of input SPL. Each curve is for a gain setting. Data above 160dB is from 7125 projector and was shifted in SPL to match with other data.....	15
Figure 5: 200 kHz hydrophone output as a function of applied gain. Each curve is for a given SPL. SPL's higher than 158 dB were obtained from the MBES projector. While no correction is needed to account for the arbitrary offset of this projector in this presentation, the labeled SPL numbers were adjusted. ....	16
Figure 6: 400 kHz hydrophone output as a function of input SPL. Each curve is for a gain setting. Data above 144 dB is from 7125 projector and has been shifted in SPL to match with other data. ....	17
Figure 7: 400 kHz hydrophone output as a function of applied gain. Each curve is for a given SPL. ....	18
Figure 8: Rapp model fitted to 200 kHz hydrophone data. Modeled curves are in bold, color lines. Data is in grey.....	21
Figure 9: Least squares fit of p-parameter of Rapp model calculated for each gain curve. Moving average excludes first point. ....	22
Figure 10: Rapp model from 200kHz data shifted by -8 dB and over-plotted on 400kHz data. Modeled curves are in bold, color lines. Data is in grey.....	23
Figure 11: 1 dB compression points calculated from Rapp model applied to 400 kHz data. (left) Output level from 7125 at calculated 1 dB compression point. (right) SPL at receiver at 1 dB compression. ....	25
Figure 12: 1 dB compression points over plotted on Rapp Model. Modeled curves are in bold, color lines. Data is in grey. The region to the left of the 1 dB compression curve has non-linear distortion less than 1 dB. The data to the right has distortion greater than 1 dB.....	25
Figure 13: 1 dB compression points calculated from Rapp model applied to 400 kHz data. (left) Output level from 7125 at calculated 1 dB compression point. (right) SPL at receiver at 1 dB compression. ....	26
Figure 14: 1 dB compression points over plotted on Rapp Model. Modeled curves are in bold, color lines. Data is in grey. The region to the left of the 1 dB compression curve has non-linear distortion less than 1 dB. The data to the right has distortion greater than 1dB.....	26
Figure 15: Beam formed data over plotted on element level model for returns from side of tank (beam 46). Beam formed data were adjusted +2.2dB vertically to compensate for beam former gain and -49dB horizontally to compensate for target strength and transmission loss. ....	33
Figure 16: Beam formed data over plotted on element level model for returns from corner of tank (beam 90). Beam formed data were adjusted -5.8dB	

vertically and -20dB horizontally to compensate for target strength and transmission loss. ....	34
Figure 17: Modeled return from various bottom types for the 200 KHz system. One symbol is plotted for each incidence angle from 0 to 64 degrees. Modeled transmit power is 220 dB (full). ....	38
Figure 18: Modeled return from various bottom types for the 400 KHz system. One symbol is plotted for each incidence angle from 0 to 64 degrees. Modeled transmit power is 220 dB (full). ....	39
Figure 19: Launch FA2806 data over plotted on tank derived model. Beam formed data has been shifted -3.5 dB to compensate for system gain and -43 dB horizontally to compensate for target strength and transmission loss. ....	44
Figure 20: Launch FA2808 data over plotted on tank derived model. Beam formed data has been shifted -5 dB to compensate for system gain and -50 dB horizontally to compensate for target strength and transmission loss. ....	45
Figure 21: Launch 2808 Plotted against modeled data for modified gains. Data has been shifted -4 dB vertically and -50 dB horizontally. ....	46
Figure 22: Launch 2807 data over plotted on tank derived model. Beam formed data has been shifted -5 dB vertically and -67 dB horizontally. ....	47
Figure 23: Nancy Foster data over plotted on tank derived model. Data has been shifted -7 dB vertically and -54 dB horizontally for gains less than 40 dB, and -64 dB for remainder. ....	48
Figure 24: Thomas Jefferson data from pier side tests over plotted on tank derived model. Beam formed data has been shifted -7 dB vertically and -55 dB horizontally. ....	49
Figure 25: Thomas Jefferson data from underway tests over plotted on tank derived model. Beam formed data has been shifted -7 dB vertically and -68 dB horizontally. ....	50
Figure 26: Segment of Nancy Foster test data showing apparent bubbles rising from mud bottom. Images are intensities of acoustic returns. Interval between images is 0.5 seconds. ....	52
Figure 27: Impact of non-linearity on backscatter. A. Output of nadir beam with increasing gain. Output signal begins to saturate at approximately 40 db of gain. B. Average angular response for each gain setting. C. Image of backscatter across swath for sequential pings. Black bands are gaps in data. Patches of different material are visible in sections with gain of 0 and 20. ....	59
Figure 28: Histograms of backscatter from 40° to 50° at increasing gain. The shape of the distribution is distorted at high gain settings. ....	61
Figure 29: Time series and frequency content of undistorted sine wave. ....	62
Figure 30: Time series and frequency content of square wave. A square wave can be seen as the limiting case for a distorted sine wave. ....	63
Figure 31: The effect of nonlinear process on sidelobe levels. ....	66
Figure 32: Sidelobe detections. Individual detection of a MBES system are shown by dots, colored by swath. Gray dots have been manually flagged as noise. These are detections on sidelobes. System was operated at full power in 5 m depth. ....	66



## **ABSTRACT**

### **LINEARITY TESTS OF A MULTIBEAM ECHOSOUNDER**

by

Samuel F. Greenaway

University of New Hampshire, December, 2010

The backscatter information available from many modern multibeam echosounder systems (MBES) has been shown to be useful for a number of purposes such as habitat classification and bottom type classification. Linearity of the system response is posited to be an important requirement for many backscatter processing techniques. A procedure to measure the system linearity is developed for the Reson 7125. These measurements are performed both in a controlled test tank environment and with systems installed on operational platforms. The linearity of the system with respect to power, gain, and the returned signal level is evaluated. It is possible to drive the Reson 7125 to nonlinear behavior. The consequences of nonlinearity on both bathymetric measurements and backscatter intensity values are developed theoretically and tested against experimental observations. Nonlinear performance generally complicates and degrades both backscatter and bathymetric data products.

## INTRODUCTION

Many modern multibeam echosounders (MBES) make two fundamentally different measurements: the detected range to a target and the amplitude of the target return or backscatter. Both measurements are made simultaneously across a swath of many, often hundreds, of individually formed acoustic beams. With the seafloor as a target, the detected range across the beams can be reduced to a set of depth measurements or soundings. Because of this ability to make many simultaneous measurements of depth, MBES systems have been in widespread use in the hydrographic community for over a decade. With their emphasis on safe navigation and charting, this community has developed models and methods to understand and verify the reliability and accuracy of the depth information derived from these systems. Concurrent to the development of MBES as efficient tools to measure depth, the amplitude information provided by these systems has been shown to be useful for a number of purposes, many related to remotely estimating the nature or composition of the seafloor. While there have been notable successes in processing backscatter data sets for various purposes, there has so far been little work on the development of requirements and practical verification methods for these data sets comparable to those that have been developed for bathymetry.

Acoustic backscatter from MBES has been shown by numerous authors to be useful through different processing approaches. Kostylev *et al.* [1] have used backscatter to classify scallop grounds in Nova Scotia. Goff *et al.* [2] investigated the use of backscatter to characterize seafloor properties of the New Jersey shelf. Sutherland *et al.* [3] used the mosaic images of backscatter to delineate areas of persistent environmental impact from aquaculture operation. These three examples show some of the diversity of backscatter applications but certainly do not span the present field. Brown and Blondel [4] give a survey of the current state of application of MBES backscatter data for habitat mapping in their introduction to the special issue of *Applied Acoustics*, "The Application of Underwater Acoustics for Seabed Habitat Mapping". In that same issue, Le Bas and Huvenne [5] offer details of common data acquisition and processing steps and compare side scan sonar systems with MBES for habitat classification. Kenney *et al.* [6] give a broader overview of seafloor mapping technologies including a broader range of acoustic and non-acoustic methods such as video cameras and cores.

Ideally, acoustic backscatter acquired for all these purposes would be geographically registered, delivered with associated high resolution bathymetry, corrected for all sonar specific parameters such as power and gain settings, and corrected for radiometric and geometric considerations [7]. If these corrections were done appropriately, the data would reflect only information about the seafloor and not the system that was used to acquire it. At present, corrections for sonar specific parameters and radiometric considerations are problematic for

multibeam systems. Multibeam sonars have been calibrated in specialized tank facilities [8]-[10]. However, removal of the installed unit is not always feasible and the system mounting environment may influence the system performance.

One common MBES backscatter processing approach is to generate mosaic acoustic images. These methods generally attempt to back out any ping-to-ping adjustments made in the systems such as power, gains, and time varied gains. The angular response of the signal is calculated and removed either through a moving average (e.g. [1]) or appropriately tuning some model (e.g. [11]) over a series of stacked pings. The resulting image can then be interpreted by trained analyst (e.g. [12]) or an image segmentation algorithm. The angular response of the seafloor that is removed in the generation of an acoustic mosaic image has been shown to contain information about the seafloor. Amongst others, de Moustier [13], deMoustier and Alexandrou [7], Hughes Clark [14], and Fonseca *et al.* [15] have demonstrated differentiation between bottom types based on various approaches to extracting the angular response from MBES data.

Another approach to seafloor classification is through the statistical distribution of the returned signal. The potential for characterizing different seafloor types through the probability density functions (pdf) of the returned echo envelope was recognized in the context of MBES by de Moustier [13] for normal incidence beams. More recent work has generalized the approach to look at the statistics at various angles of incidence [16], [17] and application of non-Rayleigh statistics for shallow water, high frequency systems [18],[19].

While the use of acoustic backscatter for seafloor characterization and habitat mapping is an area of recent and widespread interest, the calibration and quantitative evaluation of acoustic backscatter has been the subject of active interest in the fisheries acoustic community for half a century. Acoustic methods are widely used for fisheries stock assessment [20], and quantitative sonars and echo integration techniques of abundance estimation have been in use since the 1960's [21]. Standard calibration methodologies for single beam sonars [22] have been developed using spheres of known target strength and these instruments are often calibrated as a regular part of survey operations. System sensitivity, beam pattern corrections, and linearity of system performance are critical aspects of these calibrations. Recent work [8],[9] has examined theoretical and practical consideration for the applicability of MBES systems designed primarily for bathymetric surveys for quantitative fisheries studies.

Estimation of fish abundance from echo integration places strict limits on the calibrated accuracy of the sonar throughout its operating range. Non-linear performance and receiver saturation were a concern with earlier fisheries sonars and a section for testing the linearity of the receiver electronics is included in the standard calibration methodology [22]. Introduction of the Simrad EK500 and later the EK60 single beam systems eliminated this concern with very high dynamic ranges [21]. The claimed 160dB dynamic range of the EK500 was evaluated by Foote [23] through the use of specially made copper disks. This study directly showed that the measured target strength was linear over 56 dB of

dynamic range. Similar measurements of the linearity of a MBES system have not been made.

In this thesis, methods to test the linearity of a MBES are developed and implemented in a test tank environment with a Reson 7125. This system is found to be linear within most of its operating range, but departures from linearity are observed under some conditions. A model is developed to characterize the observed nonlinearity. Based on the results obtained from the tank test and a model of seafloor backscatter, conditions where this nonlinear behavior may be expected in a realistic operational situation are determined. In relatively shallow water non-linear behavior can be encountered for some portion of the returned data in all bottom types. A test of nonlinearity is developed that can be carried out with MBES systems installed on operational platforms. This test is performed on five Reson 7125 systems installed on different platforms. The results confirm the nonlinear behavior seen in the tank and allow the model of nonlinearity developed in the tank to be applied to each system. Having demonstrated that non-linear behavior can be encountered in a realistic operating environment, the implications of nonlinearities on both backscatter and bathymetry are analyzed. Depending on the method used to process the backscatter and the severity of the nonlinearity, the backscatter information can be degraded. Nonlinear system response is also shown to have an adverse impact on bathymetric data through corruption of the beam forming process. Nonlinearities are shown to increase the sidelobe levels, broaden the main beam, and lead to grating lobe like phenomenon.

## CHAPTER 1

### TANK TESTING OF A MULTIBEAM ECHOSOUNDER

In this section, the linearity of the system response of a MBES was evaluated in the test tank facility. The objective of these tests was to both establish a methodology to evaluate the linearity of a MBES system and to determine if non-linear behavior might reasonably be expected in a realistic operating environment. A Reson 7125 was used for these tests. This system is a dual frequency multibeam echosounder in widespread use by many hydrographic and oceanographic institutions. The system response was first evaluated from the element level prior to the beam forming process. This simplifies the alignment and calibration difficulties associated with narrow-beam MBES systems. The element level response is found to be nonlinear at high sound pressure levels (SPL) and high gains. A model developed for solid state power amplifiers is used to parameterize the element level nonlinear behavior. The beam formed data is also evaluated for nonlinearity. The nonlinear behavior of the beam formed data was found to be governed by the nonlinearity present at the element level. Based on the results obtained from the tank test and a model of seafloor backscatter, conditions where this nonlinear behavior may be expected in a realistic operational situation were calculated.

## **Description of the 7125 system**

The wet end of the system consists of a 200 kHz projector, a 400 kHz projector, and a dual frequency receiver. At 200 kHz, the system is capable of forming 256 beams with an across track beam width of  $1^\circ$  at nadir and an along track beam width of  $2^\circ$ . At 400 kHz, the system is capable of forming either 256 or 512 beams with a across track beam width of  $0.6^\circ$  at nadir and an along track beam width of  $1^\circ$ . With both systems the beams can be spaced either equi-angularly across the swath or equidistantly using a flat bottom assumption. At both 200 kHz and 400 kHz, the beams span 128 degrees.

While the electronic architecture of the 7125 sonar is proprietary, a general schematic of the likely superheterodyning architecture for such a system is shown in Figure 1. This model, while purely an informed conjecture, was used for the rest of this thesis to help understand the system behavior. The actual sonar architecture may have multiple intermediate frequency (IF) steps or additional components.

In the model shown in Figure 1, the hydrophone element output is passed through a fixed amplification stage and one or more variable amplification stages. The low frequency noise components are filtered out with a high pass filter. The signal is mixed with the output of a local oscillator to shift the frequency of the signal to an IF. This IF is chosen to avoid high ambient noise that may leak directly across the mixer, to allow good image frequency rejection, and is typically at a frequency where high performance filters are commercially available [24]. This IF signal is quadrature sampled to give a base banded



signal. The quadrature sampled element level signal is then processed through a time delay beam former to give the desired beam configuration.

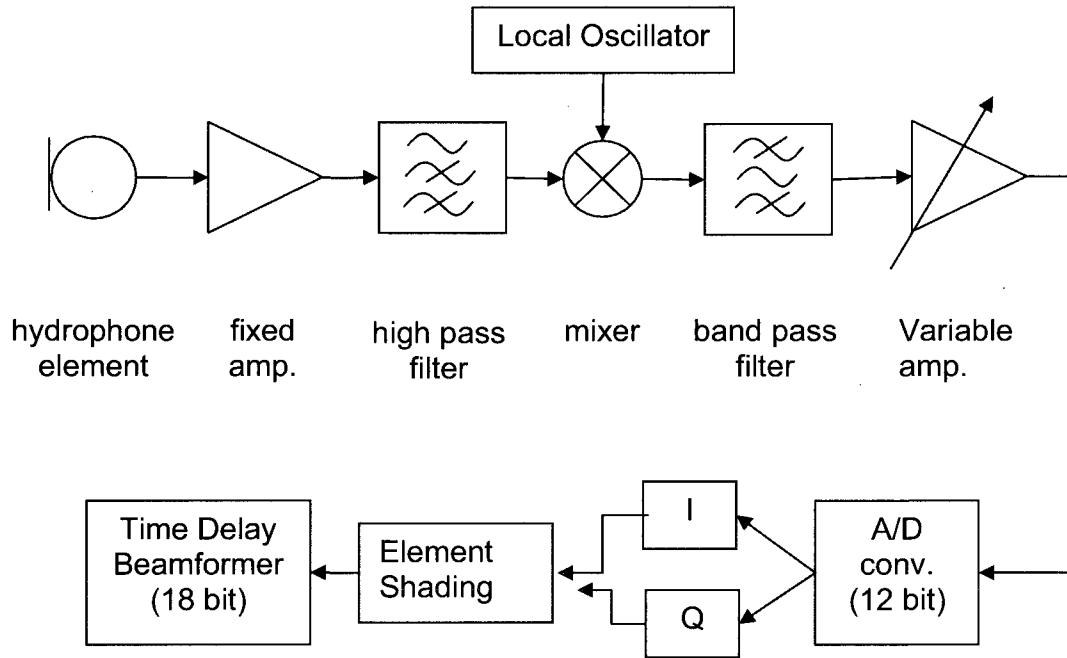


Figure 1: Assumed electronic schematic of sonar receiver

## Test Tank Acquisition

### Test Tank Configuration

For the initial test tank characterization, a Reson 7125 was mounted to a test assembly in the test tank facility at the Chase Ocean Engineering Lab at the University of New Hampshire. In addition to the series of experiments described in this thesis, a thorough characterization of the system was performed including two dimensional transmit and receive beam patterns and source and receive sensitivity levels. Details of this characterization were given by Lanzoni *et al.* [25]. A more detailed description of the development and implementation of this

test facility including characterization of three MBES systems is given by Foot *et al.* [9].

A schematic of the test tank facility is shown in Figure 2. The tank is 18 m long, 12 m wide, and 6 m deep. Two movable bridges span the width of the tank.

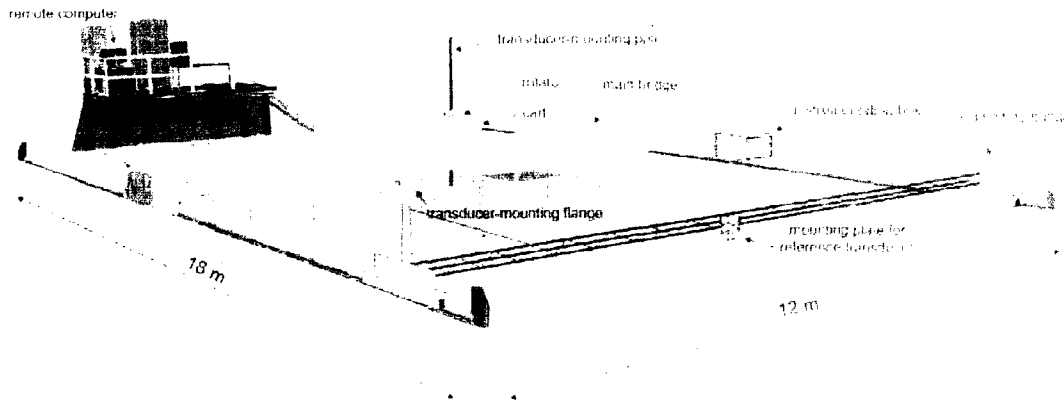


**Figure 2: Calibration Tank Facility (from Lanzoni *et al.*, 2009)**

The MBES was mounted vertically to the transducer mounting pole on the main bridge. Reference transducers were suspended from the secondary bridge. The depth of both transducers was approximately 3 m.

An Agilent 33220A 20 Mhz Function/ Arbitrary Waveform Generator was used to provide the transmitted pulse. This signal was amplified through a Krohn-Hite model 7500 power amplifier. A calibrated T/C 4034 was used to as a transmitter. A calibrated Reson T/C 4035 hydrophone was used to monitor the acoustic pulse in the water. This hydrophone output was amplified through a Stamford Research amplifier and filter. Both hydrophones were monitored with a Tektronix TDS 3014 digital oscilloscope. Connections between equipment were made with coaxial cables.

The output of the MBES was recorded on the Reson sonar processing unit. The input to the projector and the output of the reference hydrophone were monitored with the oscilloscope.

### **Linearity of Element Response with Respect to Power and Gain Settings**

A calibrated reference projector (Reson TC 4034) was mounted to a pole affixed to the secondary bridge. This projector was used to transmit a burst sine wave waveform to the MBES receiver array. The center frequency of the pulse was set to 396 kHz for the high frequency system and 200 kHz for the low frequency system. An 800 cycle burst was used for the high frequency and a 400 cycle waveform for the low frequency. This pulse length was close to the maximum length possible before the reflected multipath signal from the water surface and tank bottom began to overlap with the primary path signal. The reference hydrophone (TC 4035) was suspended from the main bridge and the spacing of the bridges and position of the reference hydrophone were adjusted until the time of flight between the source hydrophone and the MBES and the source hydrophone and the reference hydrophone were the same (to within  $1 \times 10^{-5}$  s). This distance was approximately 3.0 m. This distance is in the near field of the array if the near field is defined by the Fresnel distance [26].

$$D_{\text{array}} = \frac{L^2}{4\lambda} \quad (1)$$

Using the dimensions of the arrays, this distance is approximately 10 m for the high frequency array and 5 m for the low frequency array.

While the actual element dimensions are unknown, there are 256 elements in the HF array and 128 elements in the LF array. Assuming that the elements are adjoining, t

he near field distance of an individual element is much smaller than a meter. Thus, though the projecting hydrophone is in the near field of the array for these tests, it is in the far field of the individual array elements.

The Reson supplied engineering programs BF\_IQ.exe (high frequency) and BF\_IQ\_200.exe (low frequency) were used to control the system and record the element level data from the MBES. The output of this program is the digitized time series signal from each hydrophone. This signal is the quadrature sampled IQ pair. The sampling rate for this system is approximately 34 kHz. In accordance with the assumed electronics architecture, this signal was amplified through fixed and variable system gains, heterodyned to an intermediate frequency, and then quadrature sampled at the intermediate frequency to give a base banded signal. The MBES was used to trigger the signal generator to generate the transmitted pulse. For a particular transmit power, the fixed gain setting was increased in 1 dB steps. At each step, 10 transmit and receive cycles were manually triggered in the BF\_IQ.exe program.

The data were processed using Matlab. The amplitude of the signal was calculated as the amplitude of the complex IQ pair.

$$A = \sqrt{I^2 + Q^2} \quad (2)$$

A region of constant amplitude was selected for analysis. These selected data were away from the ends of the pulse to avoid any transient effects. An

amplitude series from two hydrophone elements, one at the center of the array and one at the end, is shown in Figure 3. The data selected for analysis are shown by the box.

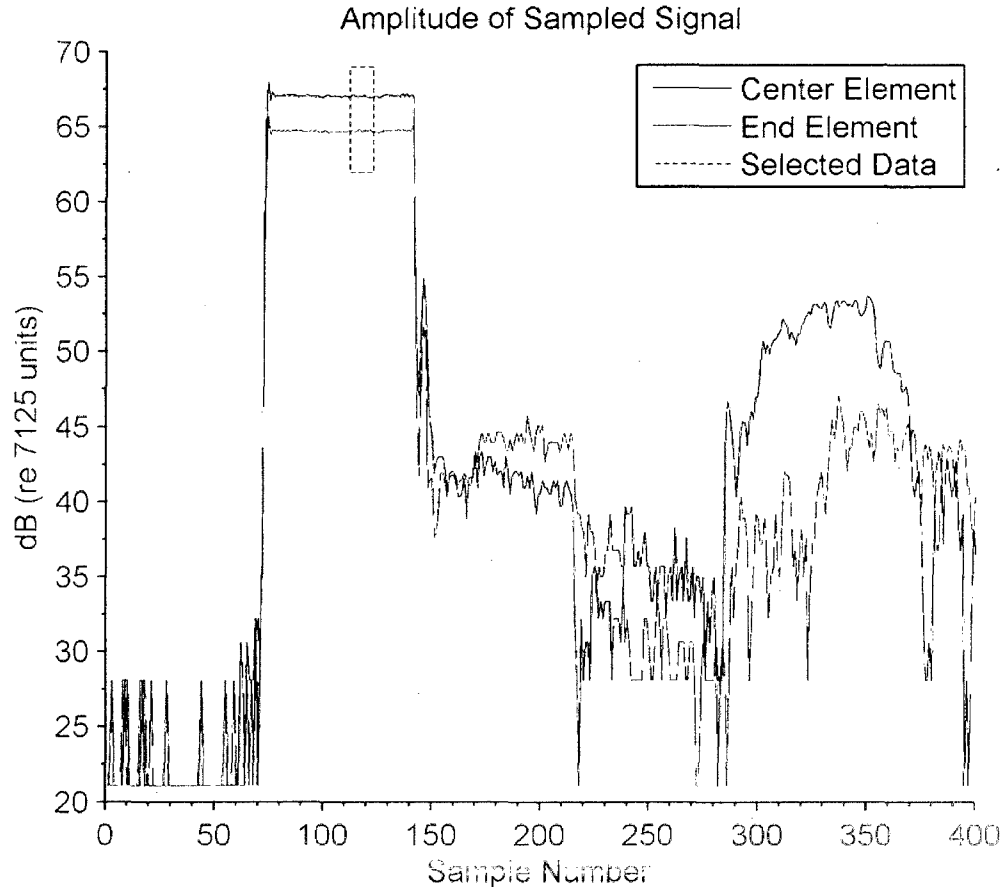


**Figure 3: Hydrophone element output. One trace is from center element of array. The other is from element at end of array. The data selected for analysis is indicated by the box.**

The root mean square (RMS) value of the selected data was calculated. This result was then averaged across all the elements. These operations were done in the linear domain prior to calculation of logarithmic levels. Because the output voltage response is assumed to be proportional to the acoustic pressure, the output level is calculated as

$$VL_o = 20 \log_{10} A \quad (3)$$

where  $VL_o$  is the output level in dB and  $A$  is the amplitude of the sampled IQ pair.

The incident sound pressure level (SPL) at the transducer face was calculated from the measured RMS voltage applied to the projector hydrophone and the known projector sensitivity, and accounting for the spherical spreading loss over the distance between the source and receiver.

$$SPL_{TX} = 20 \log_{10} V_{rms} + ML - 20 \log_{10} r \quad (4)$$

Where  $SPL_{TX}$  is the sound pressure level at the transducer calculated from the transmit voltage,  $V_{rms}$  is the measured RMS voltage to the hydrophone,  $ML$  is the projector sensitivity level and  $r$  is the distance from the projector to the receiver. The SPL measured from the reference hydrophone was also calculated from the known receive sensitivity level and the measured output voltage from the amplified hydrophone signal. This level is not corrected for spreading loss because the reference hydrophone and MBES receiver array are located at the same distance from the transmitting hydrophone and is given by

$$SPL_{RX} = 20 \log_{10} V_{rms} + ML. \quad (5)$$

The reference hydrophone was noise limited at low SPL. The transmitted voltage level was beyond the range of the monitoring instrument at the highest two SPL. The SPL valued used for analysis was taken from the transmitted level except for the two highest values, which were taken from the reference hydrophone. For SPLs above the noise floor of the reference hydrophone and below the maximum range of the monitoring instrument, the two measurements agreed to within 0.2 dB.

The maximum attainable SPL from the projector hydrophone in this configuration was approximately 167 dB (re 1uPa @ 1m). Corrected to the MBES receiver face, this gave a SPL of approximately 158 dB. To investigate the effects of higher SPL, the projector of the MBES, which is capable of a nominal SPL of 170-220 dB, was used as the transmitter. The projector was detached from the MBES mounting assembly and attached to the secondary bridge mounting pole and oriented to face directly at the MBES receiver. The separation distance between the projector and receiver in this configuration was limited by cable length to approximately 3 meters. The near field distance for the projectors calculated by the Fresnel distance was approximately 3.4m for the HF projector and 1.7m for the LF projector. A reference hydrophone was not used in this configuration because the highly directional beam pattern of the projector and near field effects would make a comparable measurement difficult. Because of the beam pattern, near field effects, and no assumed calibration for the MBES projector, the absolute value of the SPL at the receiver face was not known. This arbitrary offset was adjusted to achieve continuity with the single hydrophone data described in the previous section.

### **Tank Hydrophone Linearity Results**

The results of the tank linearity measurements are shown in Figure 4 through Figure 7. These data are shown in two presentations. One shows the curves of constant gain setting as a function of the incident SPL. The other shows curves of constant SPL as a function of applied gain. The bold curves in the higher SPL portions of Figure 4 and Figure 6 are from an independent test

where a greater number of SPL levels within the same range were investigated. At high SPL and high gain, the system response becomes nonlinear. The system response rolls off and eventually saturates. This soft roll off is termed gain compression [27] as the gain is effectively reduced at higher input amplitudes.

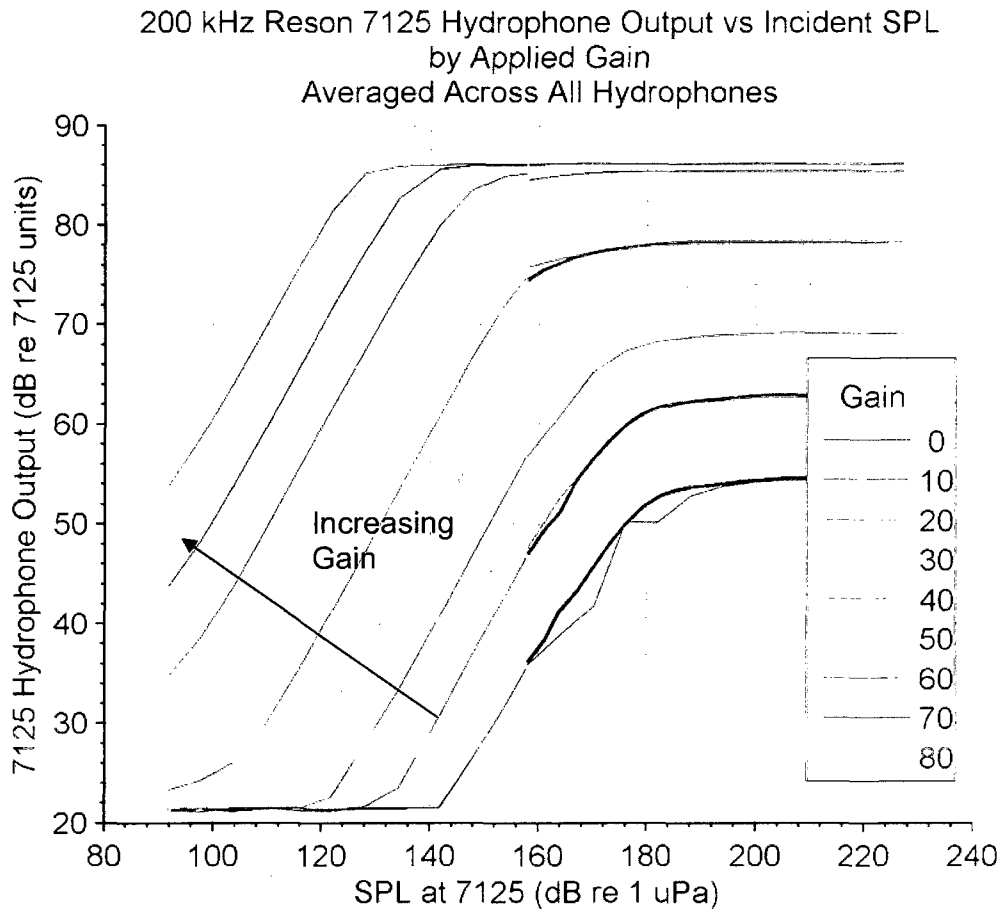
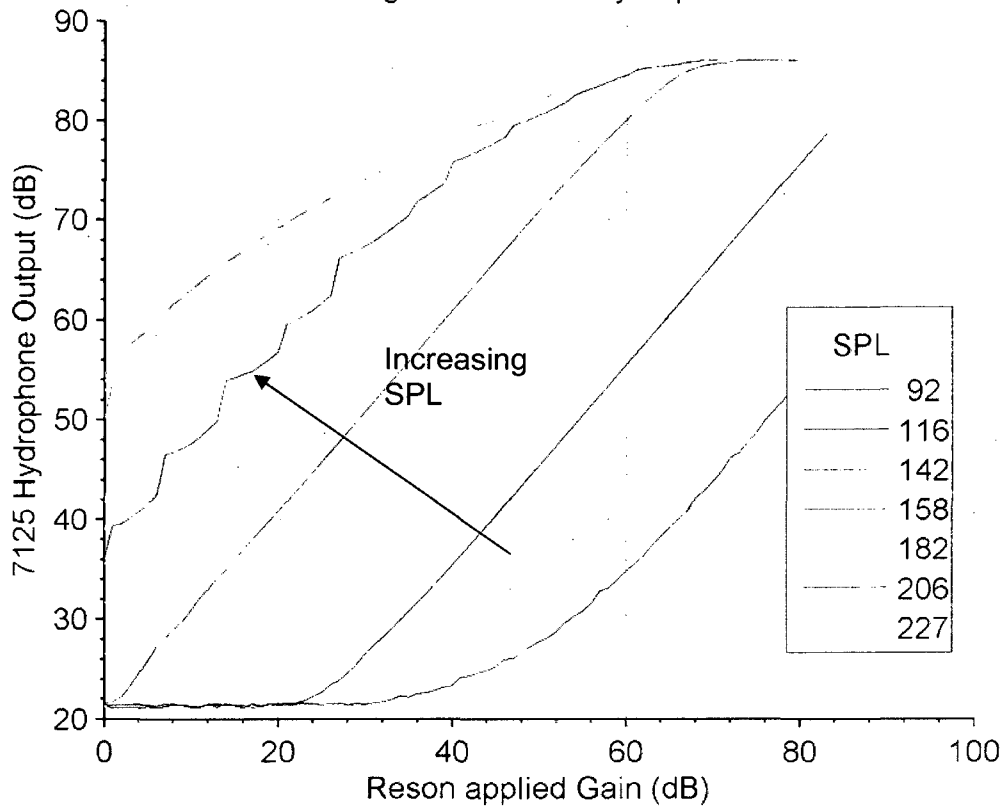


Figure 4: 200 kHz hydrophone output as a function of input SPL. Each curve is for a gain setting. Data above 160dB is from 7125 projector and was shifted in SPL to match with other data.



200 kHz Reson 7125 Output vs Gain by Applied SPL  
 by Incident SPL  
 Averaged Across All Hydrophones



**Figure 5: 200 kHz hydrophone output as a function of applied gain. Each curve is for a given SPL. SPL's higher than 158 dB were obtained from the MBES projector. While no correction is needed to account for the arbitrary offset of this projector in this presentation, the labeled SPL numbers were adjusted.**

400 kHz Reson 7125 Hydrophone Output vs Incident SPL  
 by Applied Gain  
 Averaged Across All Hydrophones

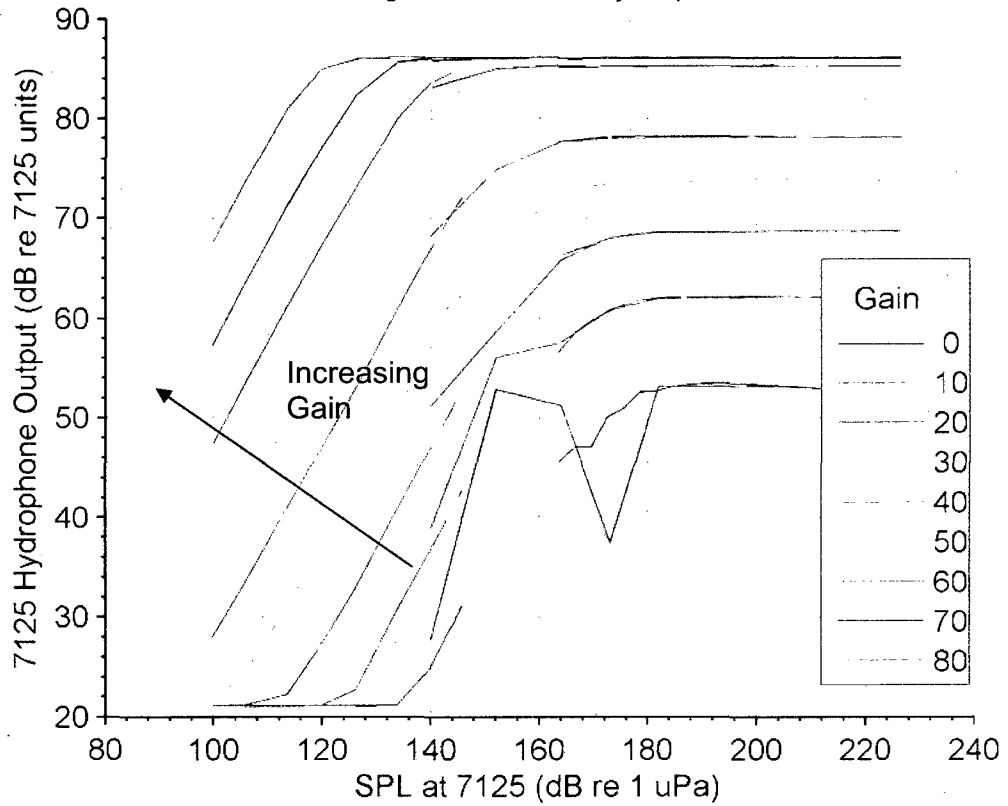


Figure 6: 400 kHz hydrophone output as a function of input SPL. Each curve is for a gain setting. Data above 144 dB is from 7125 projector and has been shifted in SPL to match with other data.

400 kHz Reson 7125 Output vs Gain by Applied SPL  
by Incident SPL  
Averaged Across All Hydrophones

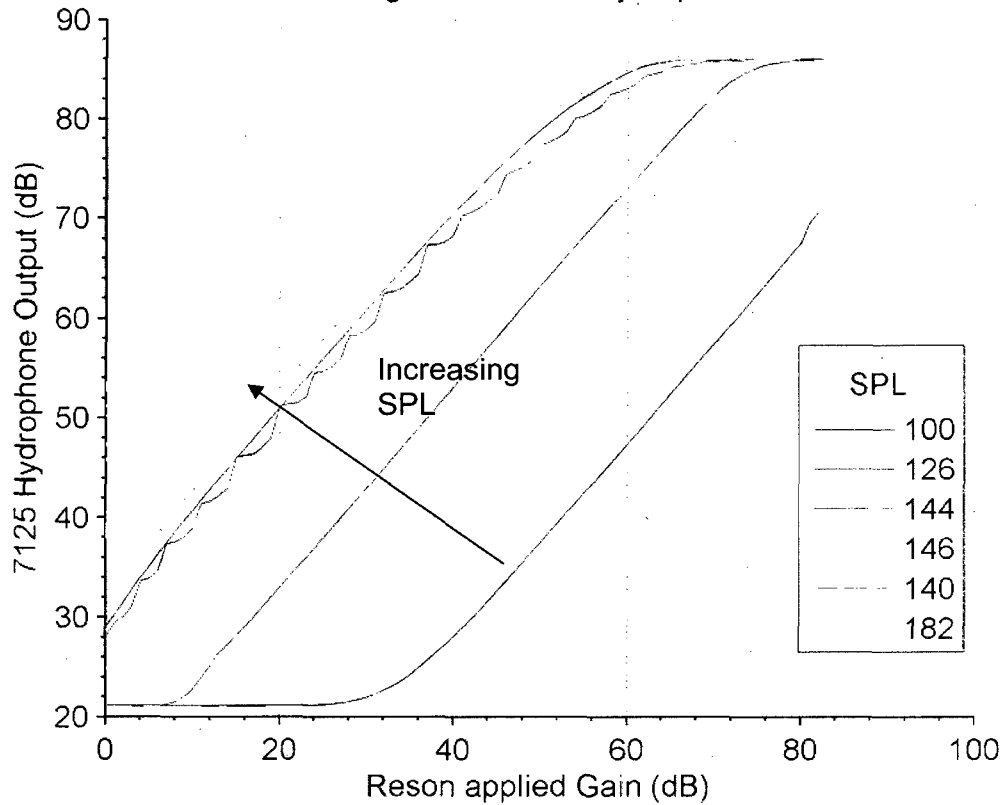


Figure 7: 400 kHz hydrophone output as a function of applied gain. Each curve is for a given SPL.

### Model Fit

The model proposed by Rapp [28] for solid state power amplifiers was used to analyze the system response. This model is given by

$$v_o = \frac{K v_i}{\left[1 + \left(\frac{K v_i}{v_s}\right)^{2p}\right]^{\frac{1}{2p}}} \quad (6)$$

where  $K$  is the small input gain,  $v_i$  is the input to the device,  $v_o$  is the device output, and  $p$  is parameter that controls the softness of the roll off. All these quantities are in linear units.

For the 200kHz system, the small input gain was extracted from the linear portion of the curves, and is the sum of the fixed system gain and the variable applied gains:

$$20 \log_{10} K = G_s + G_a \quad (7)$$

where  $G_s$  is the system gain, including the hydrophone sensitivity and any fixed gains, and  $G_a$  is the variable, user set applied gain. Then the output signal,  $S_o$ , of a linear device is given by

$$S_o = SPL + 20 \log_{10} K \quad (8)$$

and so

$$G_s = S_o - SPL - G_a \quad (9)$$

Calculating this for the linear region of the curves, the small signal system gain is:

$$G_s = -121 \text{ dB} \quad (10)$$

This is the average small signal gain of the hydrophone element chain including element sensitivity and any fixed gains. Using this value and the variable applied gain to give  $K$ , the parameter  $p$  was adjusted to best fit the data. A value for  $p$  was chosen for each variable gain setting that minimized the sum of the squares of the linear difference between the model and the data. A comparison of this model to the experimental data is shown in Figure 8. Figure 9 shows a plot of this parameter as a function of applied gain.

The same analysis was performed with the 400 kHz data. With this system, the system gain is

$$G_s = -113 \text{ dB} \quad (11)$$

or 8 dB higher than the 200kHz system gain.

Unfortunately, the data for the 400 KHz system in the region of the roll off from linear to saturated behavior shown in Figure 6 is poor. Instead of fitting the  $p$ -parameter to this data, the  $p$ -parameter for each gain setting determined from the 200 kHz system is applied to the Rapp model with the small system gain determined above. The model is over plotted on the data in Figure 10. This model closely follows the observed data to the extent that these can be evaluated.

In the proposed model of the receiver architecture, the high and low frequency systems could share all components with the exception of the hydrophone elements if the local oscillator frequency were tuned appropriately. The close match of the shapes of the curves and saturation levels suggest that the electronic architecture or perhaps the receive electronics, including non-linear effects, are in fact shared between the two frequencies. The 8 dB offset may reflect the sensitivity difference between the high and low frequency hydrophone elements or different fixed gains within the system.

200 kHz Reson 7125 Hydrophone Output vs Incident SPL  
Rapp Model

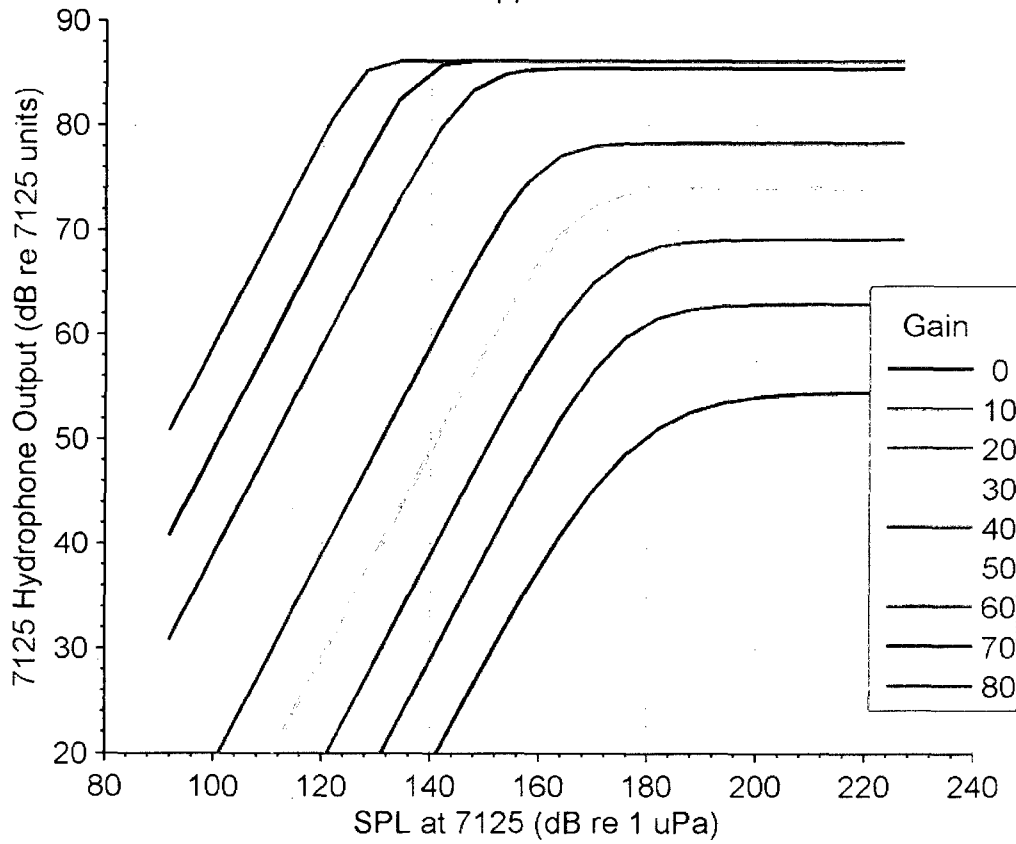


**Figure 8: Rapp model fitted to 200 kHz hydrophone data. Modeled curves are in bold, color lines. Data is in grey.**

200 kHz 7125 Hydrophone  
Rapp Model Fit

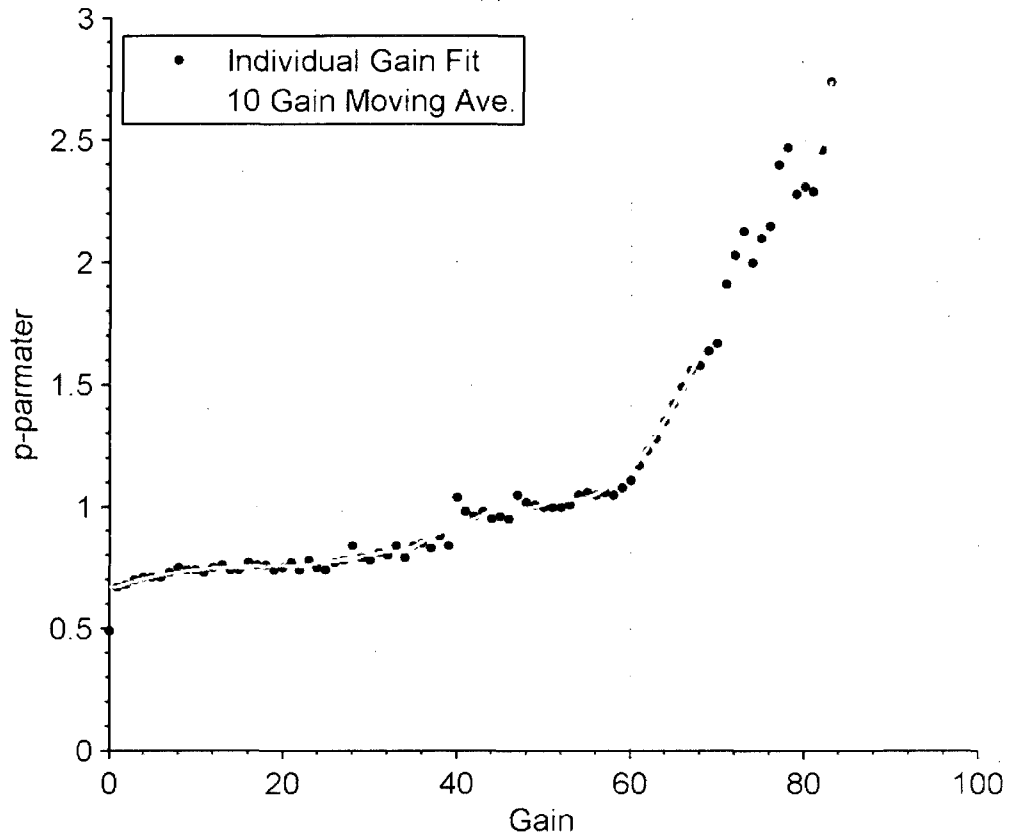


**Figure 9: Least squares fit of p-parameter of Rapp model calculated for each gain curve. Moving average excludes first point.**

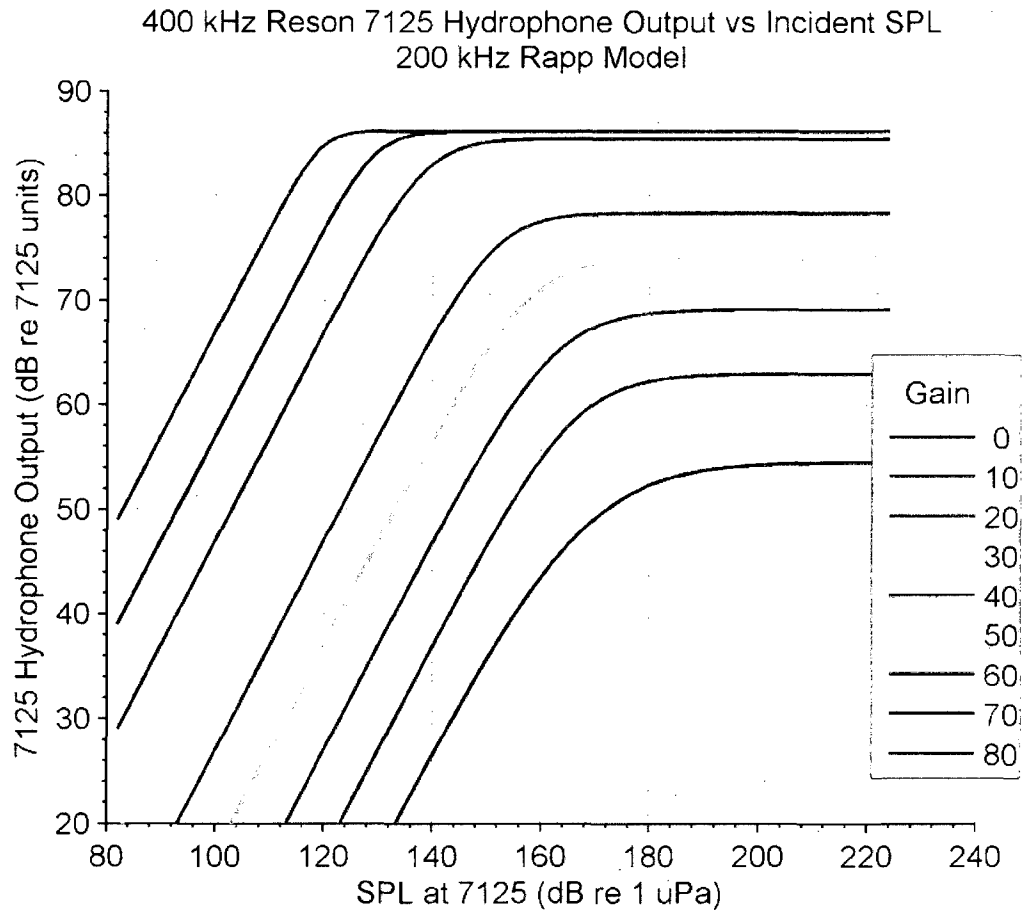


**Figure 10: Rapp model from 200kHz data shifted by -8 dB and over-plotted on 400kHz data. Modeled curves are in bold, color lines. Data is in grey.**

**Measure of Non-linearity, 1dB Compression Points**

One advantage of applying the model to the data is the deviation from linear response, or compression, can be calculated for any combination of gain and power. A measure of non-linearity in common use in electronics is the 1 dB compression point. This is the point where the output of a non-linear device is 1 dB less than the output would be if the device were linear [29]. The 1 dB compression point is convenient, but also somewhat arbitrary. The Rapp model can be explicitly solved for the 1dB compression point. The response of a linear device is



$$v_{ol} = Kv_i \quad (12)$$

Where  $v_{ol}$  is the output of a linear device,  $v_i$  is the input, and  $K$  is the gain.

Then the 1 dB compression point is given when

$$20 \log_{10} \frac{v_o}{v_{ol}} = -1 \quad (13)$$

Substituting in the Rapp model for the output and using the linear response defined above, this equation can be solved for the input value that yields the 1 dB compression points. This is given by

$$v_{i1dB} = \frac{v_s \left[ 10^{\frac{p}{10}} - 1 \right]^{\frac{1}{2p}}}{K} \quad (14)$$

The 1 dB compression point for the 200 kHz system are shown in Figure 11 and Figure 12. Figure 11 shows both the system output at the 1 dB compression point as a function of applied gain and incident SPL. Figure 12 shows the 1 dB compression points over-plotted on the system response curves. The line of 1dB compression points essentially separates the SPL gain operating space of the system into two regions. The region to the left of the 1 dB compression points (low power/ low gain) have amplitude distortions less than 1 dB. The region to the right of the 1 dB compression points (higher power/ higher gain) has amplitude distortions greater than 1 dB.

The 1 dB compression point is convenient, but also somewhat arbitrary. The impact of this distortion depends on the application. It should be emphasized that the cause of this non-linear behavior is unknown. The model used here was developed for power amplifiers, but any component, or combinations of components in the receiver could cause the observed behavior.

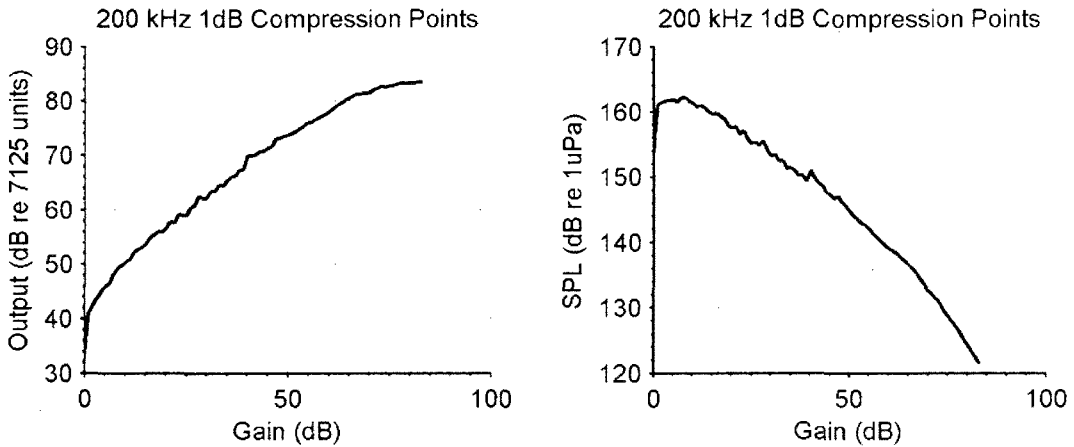


**Figure 11: 1 dB compression points calculated from Rapp model applied to 400 kHz data. (left) Output level from 7125 at calculated 1 dB compression point. (right) SPL at receiver at 1 dB compression.**

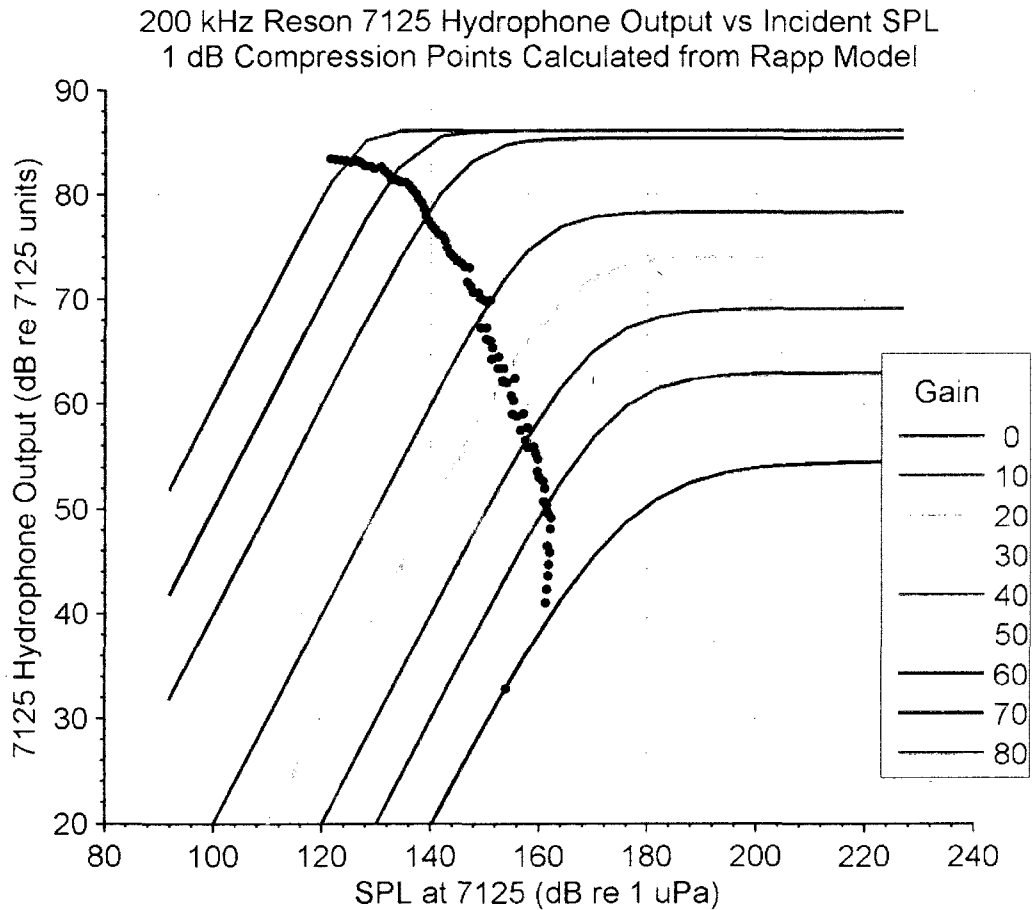


**Figure 12: 1 dB compression points over plotted on Rapp Model. Modeled curves are in bold, color lines. Data is in grey. The region to the left of the 1 dB compression curve has non-linear distortion less than 1 dB. The data to the right has distortion greater than 1 dB.**

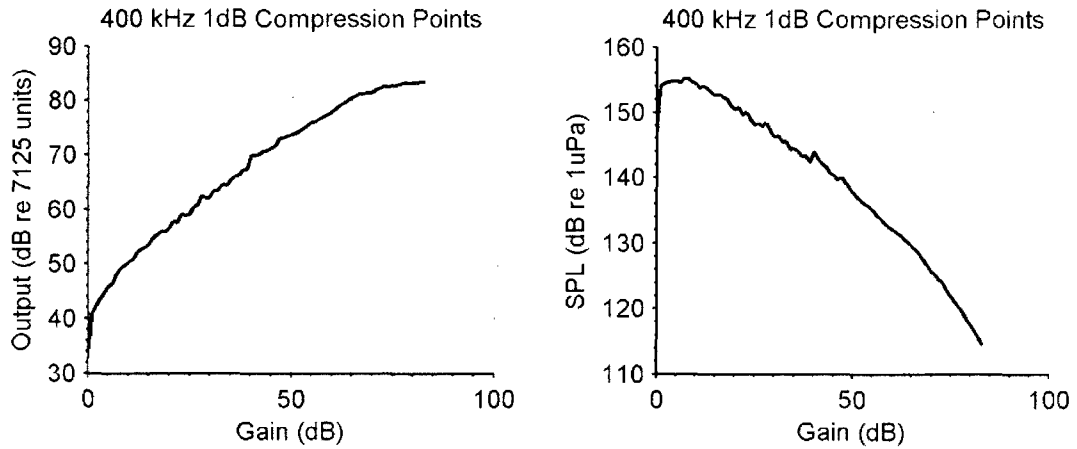


**Figure 13: 1 dB compression points calculated from Rapp model applied to 400 kHz data. (left) Output level from 7125 at calculated 1 dB compression point. (right) SPL at receiver at 1 dB compression.**

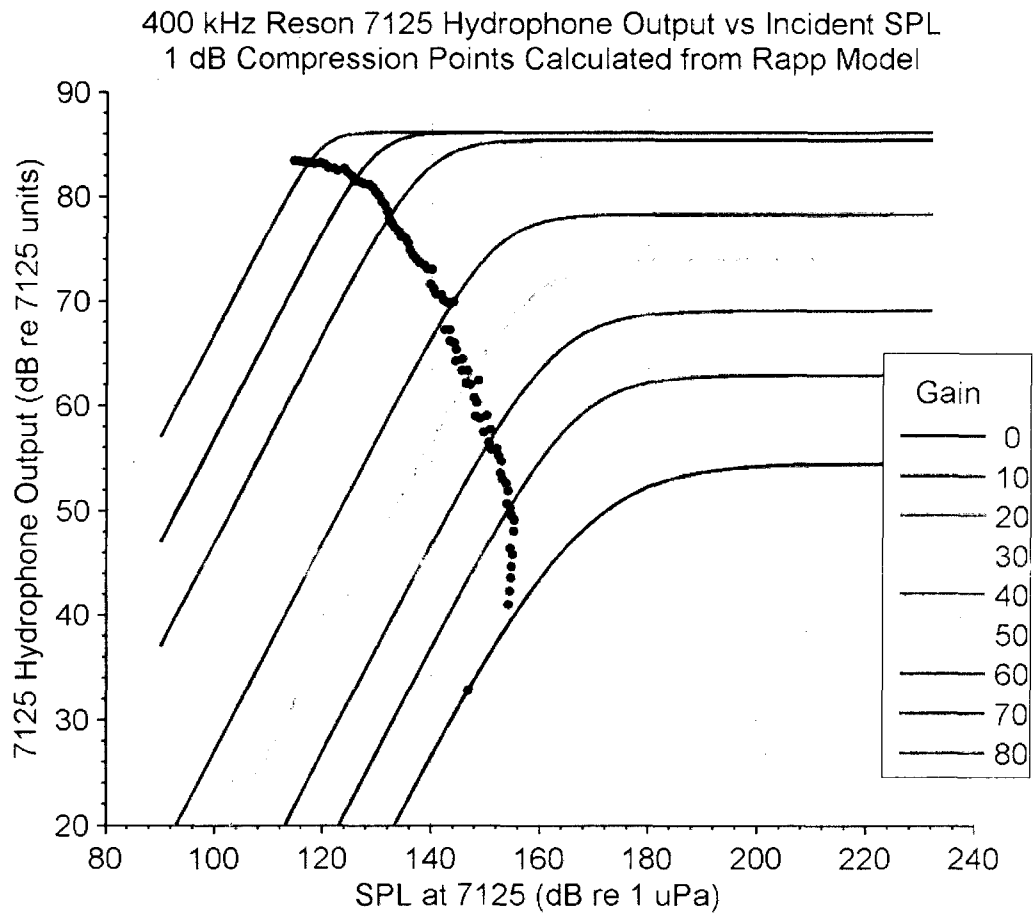


**Figure 14: 1 dB compression points over plotted on Rapp Model. Modeled curves are in bold, color lines. Data is in grey. The region to the left of the 1 dB compression curve has non-linear distortion less than 1 dB. The data to the right has distortion greater than 1 dB.**

## **Discussion**

The hydrophone level system output is linear with respect to the SPL and applied gain in a limited region of the power/ gain operation space. It is important to observe that the curves shown in Figure 4 to Figure 7 are the observed characteristics of the entire system under observation and cannot be taken as the characteristic response of any one component of the system such as an individual amplifier.

A value of approximately 21dB appears to be the noise floor of the system. The upper limit of the output level at 86 dB may be the limit of the 12 bit A/D converter. Assuming that one bit of the output is used to store the sign, an ideal 12 bit A/D converter should have a dynamic range given by

$$D = 20 \log_{10}(2^{12}) = 72 \text{ dB.} \quad (15)$$

The maximum dynamic range as determined by the maximum output value minus the minimum output value is approximately 65 dB.

Between these extreme output values, the output signal is linear for incident SPLs of less than approximately 163 dB for the 200 kHz system and 155 dB for the 400 kHz system at zero gain. For higher incident SPLs and gains, the output of the system with respect to both SPL and gain becomes non-linear and eventually saturates.

While the nonlinearity with respect to both SPL and gain may be related to the same origin in the system electronics, it is significant to note that one does not require the other. That is, saturation in the output with respect to incident SPL does not mean that the gain response must be necessarily nonlinear and a

linear gain response does not mean the incident SPL response is linear. Consider the portion of the curves shown in Figure 4 and Figure 5 for an incident SPL range of 200-220 dB and a gain range of 0-10 dB. In the region, the response with respect to incident SPL is clearly saturated while the response with respect to gain is nearly linear.

In a work detailing the effects of signal clipping on sonar array processing, Remley [30] developed the statistics of amplitude clipping in the presence of both Gaussian and sinusoidal noise. In the case of Gaussian noise, the process of clipping prior to summing across an array was shown to be equivalent to applying a soft limiter to the signal. The characteristics of the soft roll off are determined by the signal to noise ratio (S/N) and are essentially similar to the cumulative distribution of the noise. Remley's work is based on polarity processing (very hard clipping) though the analysis can be extended to a more general limiter case. This effect may lead to somewhat lower values of  $p$  (softer roll off) than might be obtained from tests of a single element at higher signal to noise ratios than was used for this test. The response curve of each element as determined above would exhibit some soft roll off, even if abruptly clipped, due to the noise in the signal when averaged over an ensemble. In addition, the average of all the elements exhibits an additional roll off due to the mismatched sensitivities of the receiver elements. However, these effects are insufficient to account for the observed roll off alone without resorting to unreasonable noise levels.

Without direct access to the component electronics, it is difficult to identify the cause of these effects. Amplifiers, mixers, and filters have all been

demonstrated to have non-linear responses, with mixers often as a limiting component in RF circuits [31].

The 1 dB compression point is a common metric of communicating the linearity of electronic components [29]. Application of the Rapp model allows the 1dB compression point to be determined directly from the model fit.

It is unfortunate that the SPL's corresponding to the region of transition from the linear region to the non-linear region were only achievable with the low end of the 7125 projector, and these measurements seem significantly more noisy than the higher levels. An omni-directional source hydrophone capable of higher output SPL than the TC 4034 would be advantageous for a better characterization.

### **Linearity of Beam Formed Response with Respect to Power and Gain**

#### **Settings**

The linearity of the beam formed data was also investigated in the test tank. The 7125 uses a time delay beam former [24]. The output of a time delay beam former with N elements is the sum of the element outputs  $s_n(t)$ , delayed by a time given by the steering angle is [26]:

$$S(\theta, t) = \sum_{n=-k}^{+k} s_n \left( t - n \frac{d}{c} \sin\theta \right) \quad (16)$$

Where d is the spacing between elements, c is the sound speed, and n is the element number. In this case, the time delays are referenced from a central element in the array, so the total number of elements is

$$N = 2k \quad (17)$$

In practice, because the required time delays are generally not equal to the sampling interval, some interpolation is required [26]. A comprehensive review of the subject of fractional time delays is given by Laasko [32]. For the present purposes, it is sufficient to note that the time delay beam forming process is a linear function of  $s_n$ . Thus, the output of the beam former should be linear with respect to power and gain if the individual elements are linear and the non-linear characteristics of the beam formed data should reflect the nonlinearity of the element level data. However, the beam former may have some linear performance limit that may limit the overall system linearity. If for instance, the beam former is implemented with 18 bit architecture, a sum across the elements that is larger than 18 bits will be clipped.

The MBES was suspended from the main bridge approximately 3m from one end of the tank and was oriented to face the long dimension of the tank. In each test, the gain was held constant as the power was increased through all settings (nominally 170 to 220 dB). This was repeated for gain intervals of 10 dB from 0 to 80 dB. The beam formed water column data were recorded in the Reson .s7k format. A selected target area was manually designated across a number of beams and samples, and the maximum signal level within that area was extracted.

The technique of extracting the maximum within the window was motivated by the dynamics of the field acquisition method discussed in the next section, but has been included here for consistency. In the tank environment, there is no discernable difference in the results between extracting the maximum

within the window and carefully selecting the individual sample and beam number corresponding to a particular target initially; in the tank, the maximum return within a spatial window comes from the same beam and sample number from ping to ping. However, in a field environment, such precise control of the relative positions of the target and MBES is not possible. The method of extracting the maximum from within the window is far simpler to implement than *correcting for vessel motion and beam patterns*. This technique is similar to that proposed by Cochrane *et al.* [8] in discussions of target strength extraction from MBES data.

To compare the beam formed results to the element level results shown in the previous section, it is necessary to compensate for the source level of the transmission (SL), the round trip transmission loss (TL), and the target strength (TS) of the target, with all levels referencing logarithmic quantities. In general, the SPL at the receiver face will be given by

$$SPL = SL - TL + TS \quad (18)$$

For this experiment, it was assumed that SL was linear with respect to the transmit power setting (TPS) of the system. For any given target, it was also assumed that TL and TS were independent of SL, which is generally true for small signals. The returned SPL for a fixed target is given by the transmit power setting (TPS) plus some unknown constant (C) that is a function of range and the particular ensonified target.

$$SPL = TPS + C \quad (19)$$



The gain (in dB) of the beam former will also generally be non-zero. In the following plots the beam formed data for a particular target were manually adjusted by adjusting the horizontal offset to adjust for the combined effects of target transmission loss and vertically to adjust for beam former gain.

The results for two target areas are shown in Figure 15 and Figure 16. Unfortunately, the 400 kHz results were recorded with a time varied gain applied. Because the exact gain applied at each sample is unknown, a presentation of these data in a comparable sense was not possible.

In the following plots, the 200 kHz beam formed data were plotted over the Rapp model derived from the hydrophone data. To accommodate the unknown beam-former gain, the data were vertically shifted *en bloc*. To accommodate the unknown target strength and transmission loss, the data were horizontally shifted. Both shifts were done visually to best fit the bulk of the data.

200kHz Reson 7125 Hydrophone Output vs Incident SPL  
 by Applied Gain  
 Averaged Across All Hydrophones

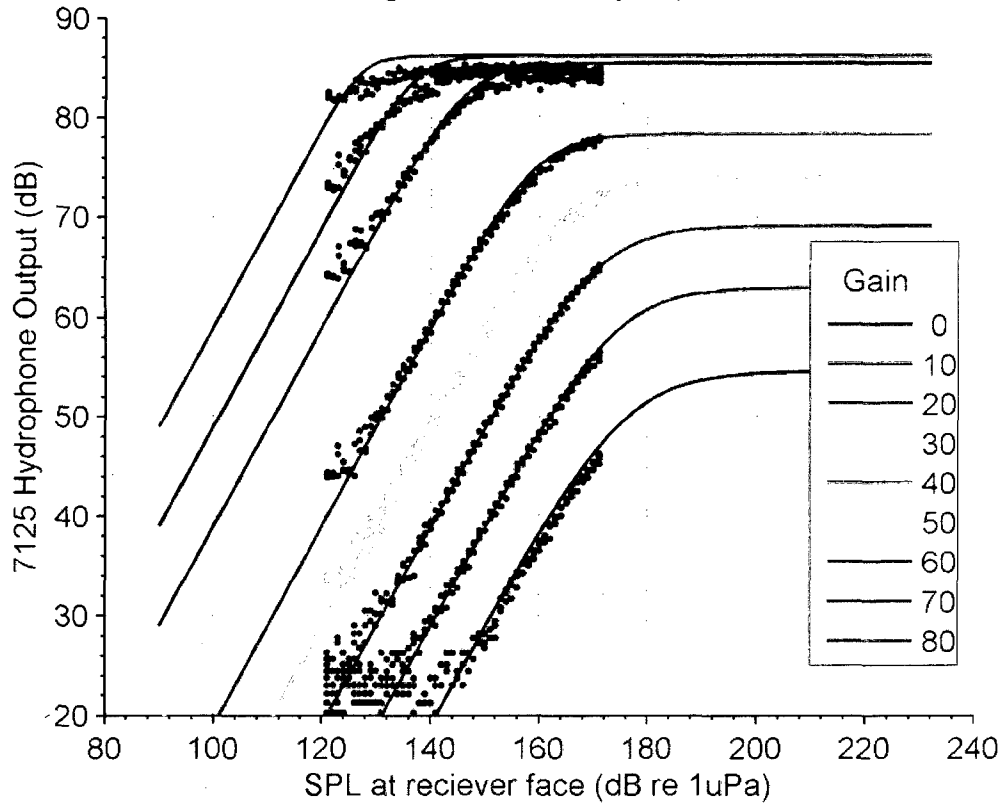


**Figure 15: Beam formed data over plotted on element level model for returns from side of tank (beam 46). Beam formed data were adjusted +2.2dB vertically to compensate for beam former gain and -49dB horizontally to compensate for target strength and transmission loss.**

200kHz Reson 7125 Hydrophone Output vs Incident SPL  
by Applied Gain  
Averaged Across All Hydrophones

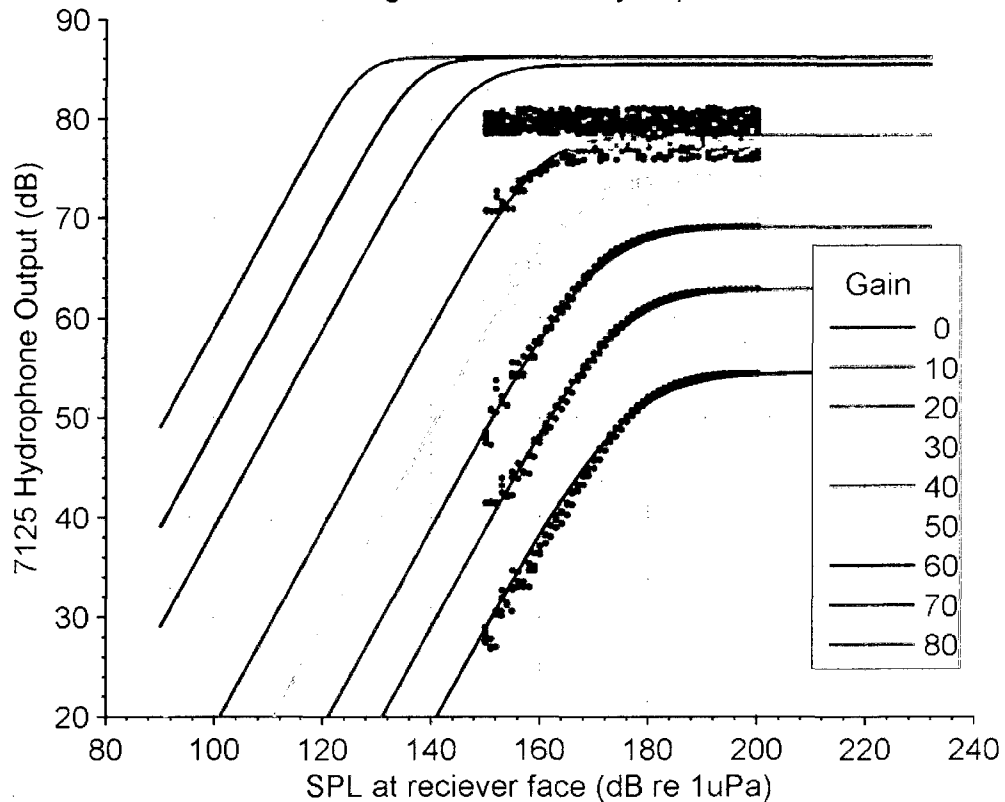


**Figure 16: Beam formed data over plotted on element level model for returns from corner of tank (beam 90). Beam formed data were adjusted -5.8dB vertically and -20dB horizontally to compensate for target strength and transmission loss.**

### Discussion

The beam formed data show similar saturation characteristics as the element level data. After shifting the beam formed response data *en bloc* to compensate for the unknown beam forming gain and target strength, the shape of the response curves closely matches that of the element level response. This indicates that the nonlinear behavior of the beam formed data is due solely to the nonlinear behavior of the element level responses. Due to the low directivity of

the individual elements and the short near-field distance when compared to the array, the element level response is far simpler to calibrate than the full array.

For the beam formed data, if the transmit source level was known and transmission loss was reliably estimated, this fitting process could yield a direct estimate of both the target strength and the gain of the beam forming process. As long as there is sufficient shape in the curves of response vs. SPL, ideally with both a linear segment and one at full saturation, TS and beam former gain can be independently estimated. Recognizing that the low directivity of the individual elements makes the element level calibration not particularly sensitive to alignment of the source with the receiver, this technique could be useful in a field environment where such alignment is problematic for narrow beam systems. The stability of the saturation points and beam former gain are not known.

### **Prediction of Returned SPL and the APL-UW Model**

From the previous tests, it is clear that to drive the system into a non-linear response requires either a high gain value or high incident SPL at the receiver face. The high gain non-linearity or clipping might be the easier of the two to monitor by an operator. If the output value of the system is at or near the maximum values attainable by the system, then this clipping is occurring. The high SPL non-linearity effect might be more difficult to monitor during acquisition because the value of any particular amplitude alone does not give sufficient information to evaluate linearity. The saturation curves of the particular system must be known as well as the returned signal and the system gain (including time varied gain) that has been applied to the returned signal. Without this

information, this non-linearity is not immediately evident in recorded data based solely on the on the recorded intensity values. As an example, consider the data shown in Figure 16. At a fixed gain setting of zero and an incident SPL of 200, the system output is approximately 52 dB, well below the maximum output of approximately 82 dB. At this point however, the receiver is clearly fully saturated with respect to SPL at the operating point. Any monitoring of the output signal level alone is insufficient to monitor for this saturation.

To evaluate if the returned signal levels might be high enough for high SPL nonlinearity to be a concern in a realistic field environment, the returned signal levels from a variety of seafloors were modeled. The returned sound pressure was calculated as

$$SPL = SL - 40 \log_{10} R - 2 \alpha R + BS + 10 \log_{10} A \quad (20)$$

where SL is the source level, R is the slant range,  $\alpha$  is the absorption coefficient, BS is the backscatter strength, and A is the ensonified area [26].

The APL-UW model [33] was used to give the angular backscatter response of the modeled seafloor. A flat bottom assumption was used, and the ensonified area was taken to be the smaller of the pulse length limited or beam width limited footprints. Because the returned SPL at the transducer face drives the linear behavior, the receive beam pattern generated by the beam forming process can be neglected. The element level beam pattern is assumed to be omni-directional for this calculation.

In this model, the transmission loss followed spherical spreading and linear absorption. The absorption constant was 0.11 dB/m for 400 kHz and 0.50

dB/m for 200 kHz. These are the recommended default salt water settings for the system recommended by the manufacturer [34].

The total applied gain is required to model the receiver response. This total gain is the sum of fixed and time varied gain (TVG). Presumably to accommodate limited dynamic range in TVG, Reson applies a TVG function that departs somewhat from the  $30\log R$  plus absorption that might be expected for use with bottom returns. Reson provided a MATLAB function for calculating the applied gain from a system that had been gain calibrated. After removing the fixed system sensitivity that was embedded in this function, this information was used to calculate the gain applied to the signal for a given fixed gain, absorption, and spreading coefficients.

The output of this backscatter model is input into the Rapp model developed in the previous section. This result is shown in Figure 17 for the 200 kHz system and Figure 18 for the 400 kHz system. For each of the seven bottom types shown, the output signal level from the Rapp model was calculated for each degree of incidence angle from 0 to 64 degrees. While this does not correspond to the number of beams in this system, it does give an indication of the system performance across the swath. The 1dB compression points were calculated from the smoothed  $p$ -parameter and are over plotted as a dashed line on the figures.

200kHz Reson 7125 Hydrophone Output vs Incident SPL  
 Overlay with SPL from APL-UW backscatter model  
 Water Depth: 10m  
 TVG paramters: Abs: 0.05, Spread: 30 Fixed Gain: 10

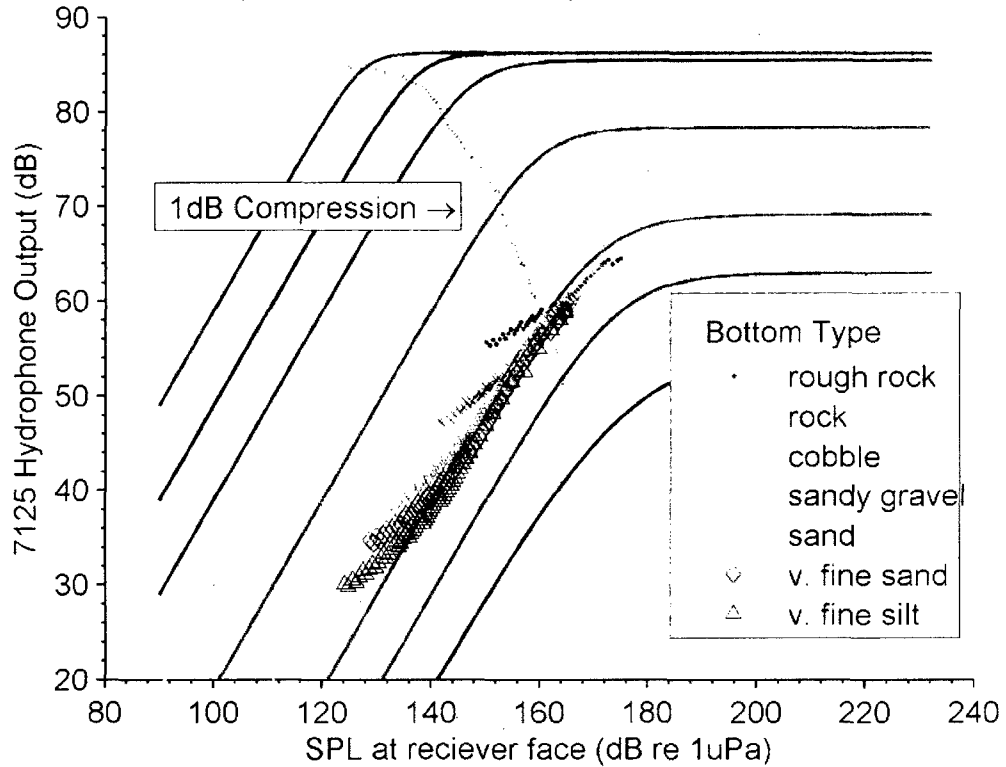


**Figure 17: Modeled return from various bottom types for the 200 KHz system. One symbol is plotted for each incidence angle from 0 to 64 degrees. Modeled transmit power is 220 dB (full).**

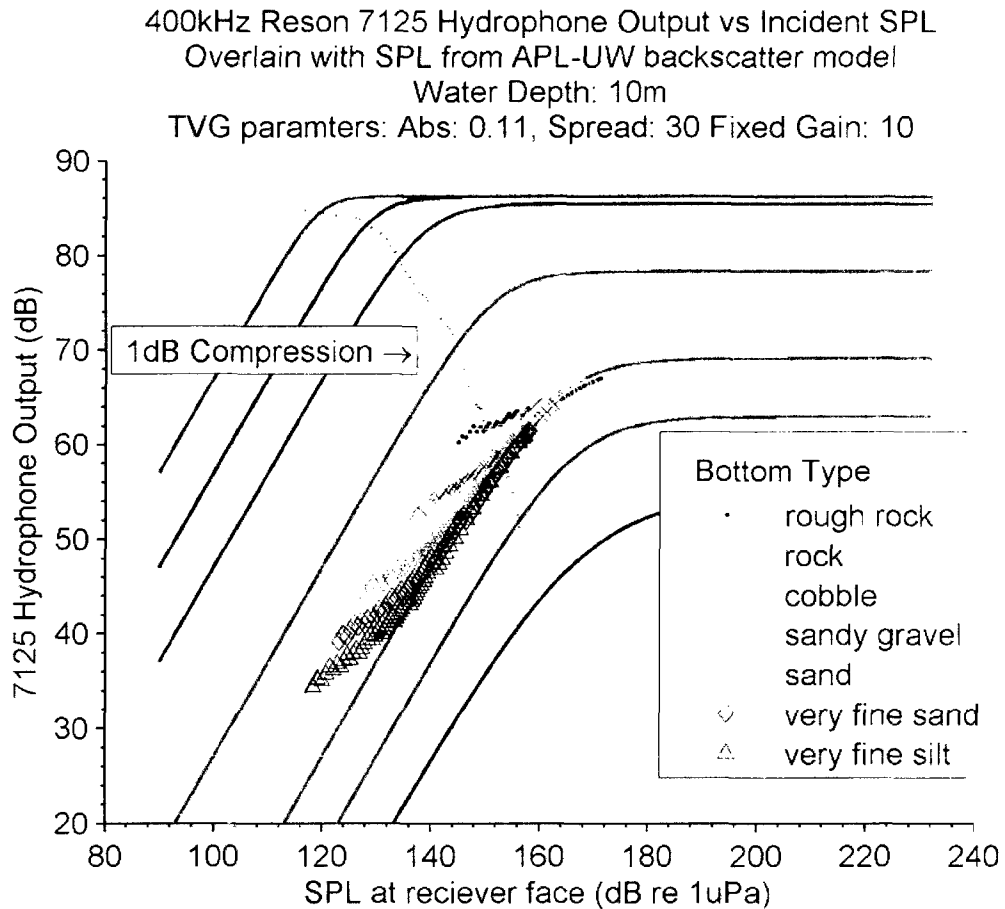


**Figure 18: Modeled return from various bottom types for the 400 KHz system. One symbol is plotted for each incidence angle from 0 to 64 degrees. Modeled transmit power is 220 dB (full).**

### Discussion

The modeled seafloor response indicates that it is possible to drive the system beyond the linear operating region of both the 200 kHz and 400 kHz systems under reasonable operating conditions in shallow water. At full power in 10 m of water, the nadir returns are in the non-linear response regime for all bottom types. In shallower water, the returned signal level would be higher still and the nonlinearity more pronounced. For a rough rock bottom type at 400 kHz, the system is operating in the nonlinear regime across most of the swath.



The differences between the two operating frequencies are a combined result of: the different modeled responses of the seafloor at the two frequencies, the different projector beam width, and the different sensitivities of the two systems. The two figures do show that for a given depth of water and bottom type and the same operating parameters, more of the swath is nonlinear with the 400 kHz than the 200 kHz system.

These figures can be used to predict the changes in the operating parameters required to bring the system performance into the linear regime. For example, when operating the 400 kHz system in 10 m of water over a rough rock bottom, the SPL at the receiver face at the nadir return is the strongest and is at the farthest right of the point plotted on Figure 18. The SPL value of this modeled return is approximately 20 dB greater than the 1 dB compression value for that gain setting. To bring the system into the linear operating range across the swath, the transmit power must be reduced by 20 dB to 200 dB.

This result is only strictly valid for the system that the model was derived from in the tank. A different system may have different sensitivities or electronic performance.

## CHAPTER 2

### FIELD TESTING OF A MULTIBEAM ECHOSOUNDER

In this section, the linearity tests performed in a controlled tank environment are generalized for use in the field. The modeling of the seafloor response with the results from the tank characterization showed that nonlinear behavior of the Reson 7125 could be encountered under plausible operating conditions. The tests in this section confirm that conclusion. In addition, comparison of the field test results with the Rapp model allows the gain compression of the tested unit to be evaluated in the output units of the sonar.

The beam formed linearity test discussed in previous section was performed in a field environment with five 400 kHz Reson 7125 units mounted on different survey vessels. These tests were opportunistic and illustrate that under some conditions, results similar to those obtained in the controlled test environment can be obtained in an operational setting. In other cases, environmental conditions may preclude a successful measurement.

The installed units were all on NOAA survey vessels. All tests were performed while the vessels were stationary. In one case, the vessel was stopped at sea for an oceanographic cast. In the other cases, the vessel was tied up to a pier.

The installations and test environments are summarized in Table 1. The NOAA Ship *Thomas Jefferson* is a hydrographic survey ship. The MBES is in a fixed hull mount near the bow of the vessel. Test data were acquired in two locations. The first location was in Block Island Sound off the coast of Rhode Island while the vessel was stopped. The second location was alongside the ship's home pier in Norfolk, VA. FA 2806, FA 2807, and FA 2808 are hydrographic survey launches carried by the NOAA Ship *Fairweather*. The MBES are in a fixed hull mount near the center of the vessel. Test data were acquired alongside the pier at the NOAA Western Regional Center. The NOAA Ship *Nancy Foster* is a mapping and research vessel. The MBES is mounted to a pole in a moon pool. Data were acquired alongside the ship's home pier in Charleston, SC.

**Table 1: Field Linearity Measurements**

Test	Vessel	Vessel Length (m)	Depth below transducer (m)	Bottom Material	Test Location
1	Thomas Jefferson	63	30	Sand	BI Sound, RI
2	Thomas Jefferson	63	6	Mud	Norfolk, VA
3	FA 2806	9	5	Rock	Lake Washington, WA
4	FA 2807	9	10	Silt	Lake Washington, WA
5	FA 2808	9	10	Silt	Lake Washington, WA
6	Nancy Foster	56	6	Mud	Charleston, SC

In all cases, the data were acquired directly from the Reson 7k processor in the Reson .s7k format. The pulse repetition rate was set to 10 pulses per

second (PPS) to reduce multipath echoes. Beam formed, full water column data were continuously recorded as the power was slowly increased from off to maximum at a particular gain setting. The fixed gain was increased by 10 dB and the power was lowered slowly to off. This was repeated until the full range of power and range settings was spanned. Each test required approximately 10 to 15 minutes to acquire.

The processing was done using Matlab. The data were visually inspected to determine the bottom location. A box was defined around the nadir region and the maximum amplitude value within that box was extracted. As with the tank tests, the transmit power setting was assumed to be related to the incident SPL at the receiver by a constant dB offset that accounts for the target strength and transmission loss as in (18) and (19).

The beam formed data were shifted *en bloc* to best match the model derived from the tank measured element level response discussed in the previous section. Because these tests used different MBES units, the element level system response can no longer be assumed to be common with that measured in the tank. The vertical shift applied to the data then included the beam former gain as well as the difference in the average element level sensitivity between the two units. The horizontal offset still encompasses both the transmission loss and the unknown target strength of the seafloor target.

The results for five of the tests are shown in Figure 19 to Figure 25 below. The data from launch FA2806 were acquired in approximately 5m of water over a mixed rocky and silt bottom and is shown in Figure 19. The data were adjusted

vertically by -3.5 dB to compensate for both beam former gain and the sensitivity difference of this system, and horizontally by -43 dB to compensate for both the transmission loss and target strength of the seafloor. Following adjustment, the data generally match the model derived from the tank measured element level response. High SPL non-linearity is observed at all gain settings.

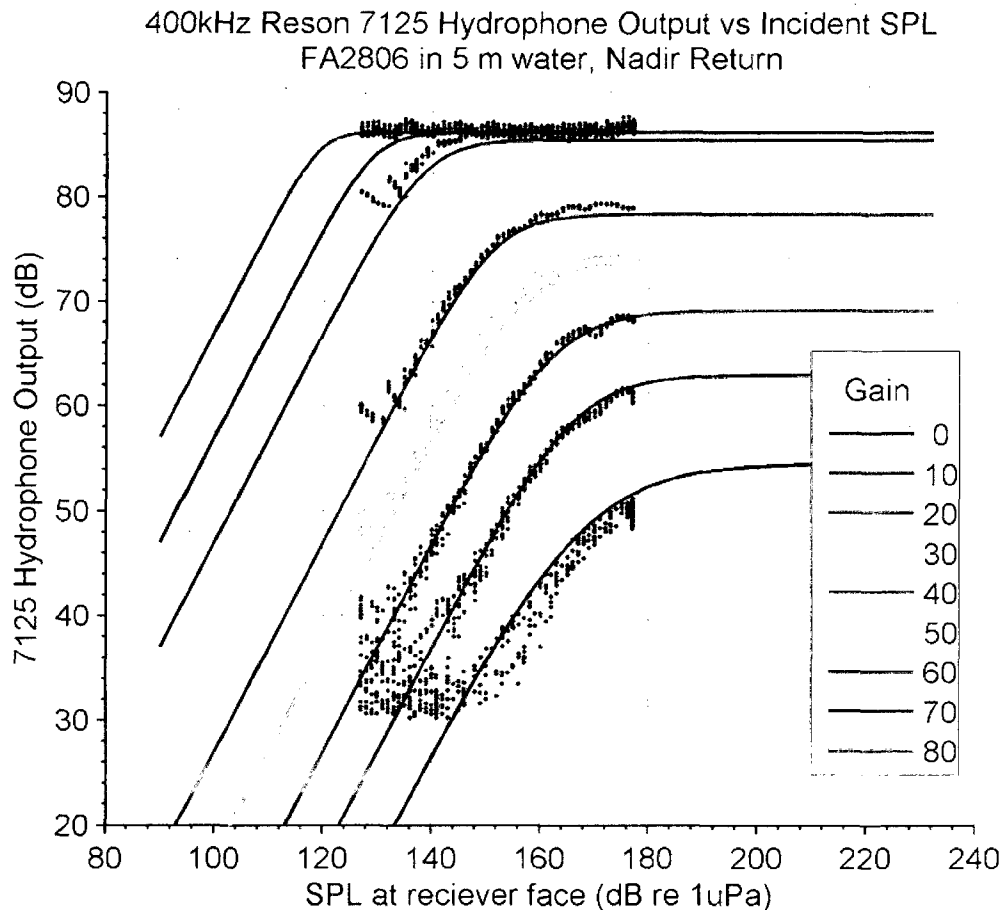


**Figure 19: Launch FA2806 data over plotted on tank derived model. Beam formed data has been shifted -3.5 dB to compensate for system gain and -43 dB horizontally to compensate for target strength and transmission loss.**

The data from Launch FA2808 were acquired in approximately 10m of water over a silt bottom and is shown in Figure 20. The data were adjusted -5dB vertically to compensate for both beam former gain and the sensitivity difference of this system, and horizontally by -50 dB to compensate for both the

transmission loss and target strength of the seafloor. Following adjustment, the data show similar roll off effects as the modeled response curves, but do not agree in gain spacing. Increasing the gain setting of this system by 10 dB increases the output by approximately 1.1 dB. Figure 21 shows the data over plotted on curves modeled with this modified gain. In this plot, the data acquired with a gain setting of 10 are compared with the modeled response at a gain of 11 and so on.

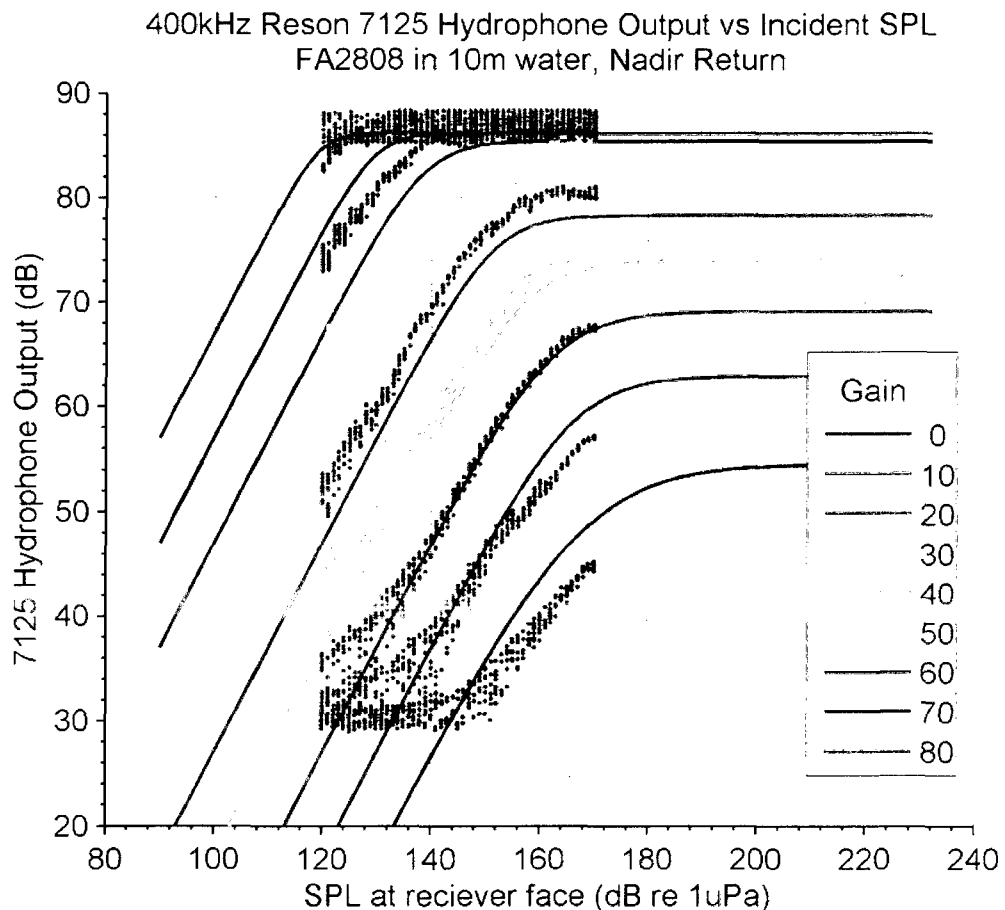


**Figure 20: Launch FA2808 data over plotted on tank derived model. Beam formed data has been shifted -5 dB to compensate for system gain and -50 dB horizontally to compensate for target strength and transmission loss.**

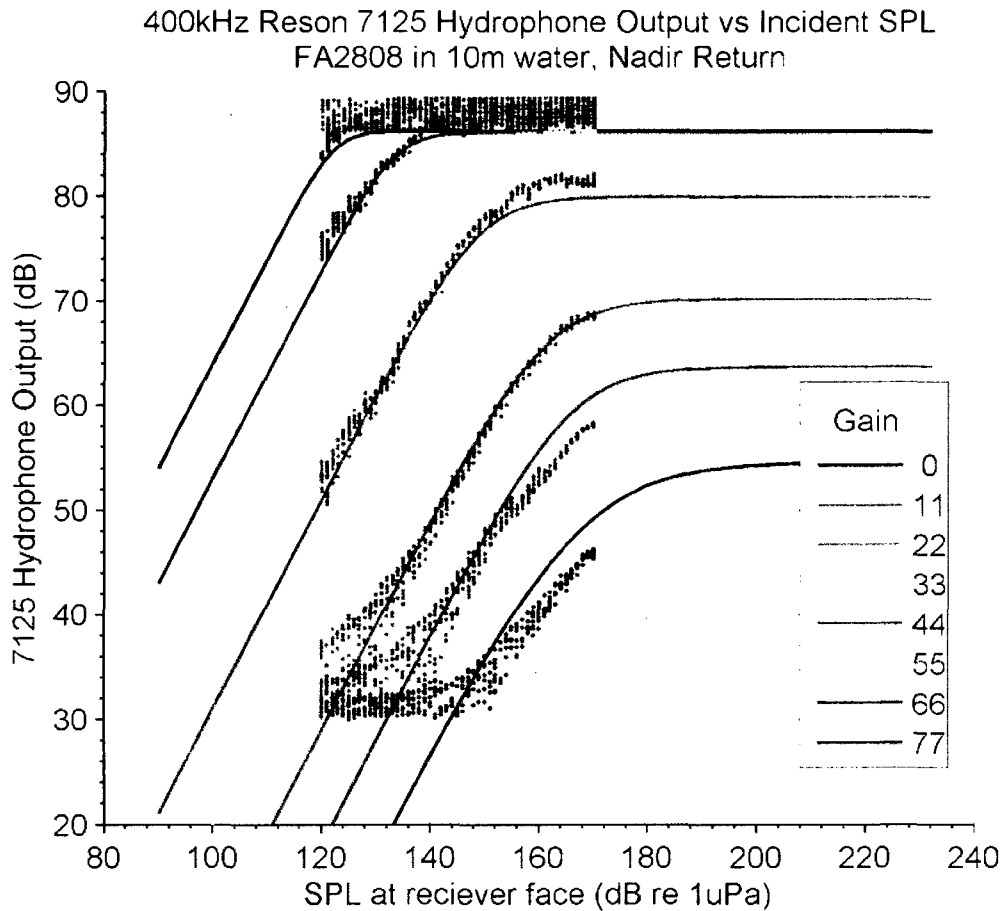


**Figure 21: Launch 2808 Plotted against modeled data for modified gains. Data has been shifted -4 dB vertically and -50 dB horizontally.**

Assuming that the actual gain applied to the system is 1.1 times the gain setting yields a closer match to the model, though at high SPL's there is some deviation from the model shape. High SPL non-linearity is observed at most gain settings.

The data from Launch FA2807 were acquired in approximately 10 m of water over a silt bottom and is shown in Figure 22. The data were adjusted -5dB vertically to compensate for both beam former gain and the sensitivity difference of this system, and horizontally by -67 dB to compensate for both the transmission loss and target strength of the seafloor. While the gain increments of FA2807 appear to be generally in line with the model, this unit showed what

appeared to be anomalously low sensitivities. In the same conditions as 2808, over approximately the same target bottom and in the same depth of water, the maximum returned SPL levels are approximately 15 dB lower than the system on FA2808. This was later found to be a result of the high and low frequency projectors being swapped on the boat. This was rectified prior to operational use.

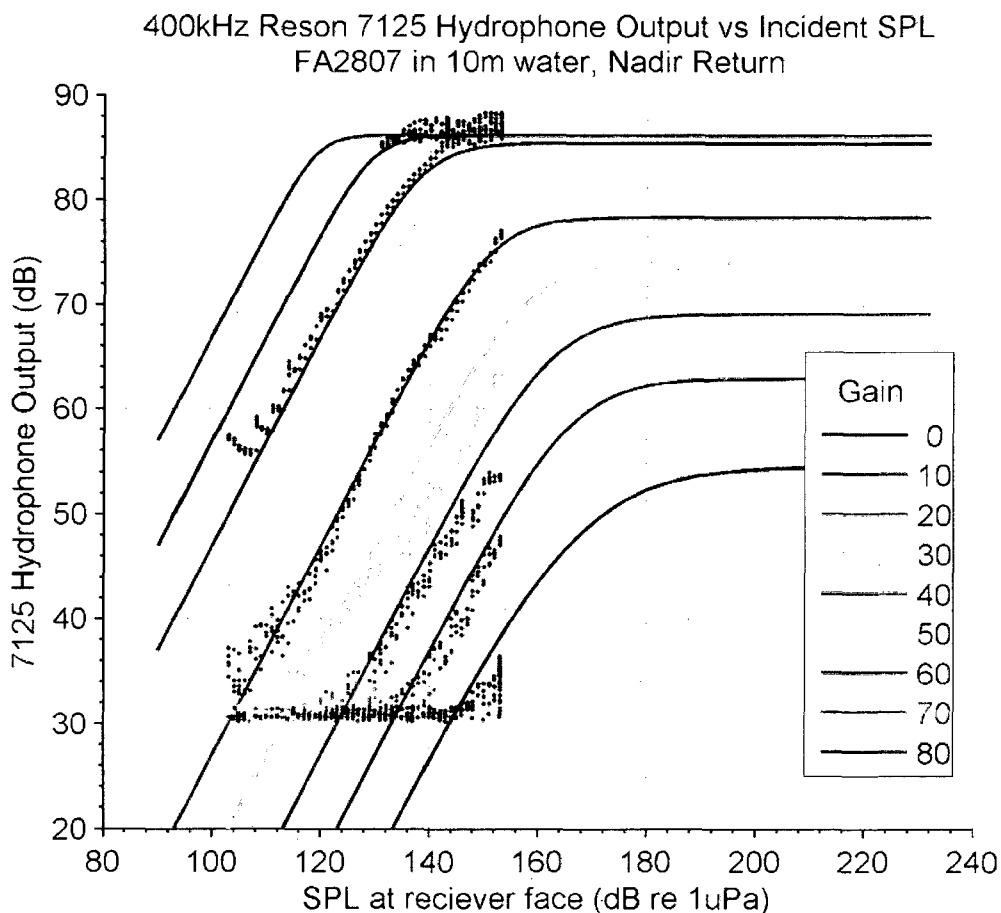
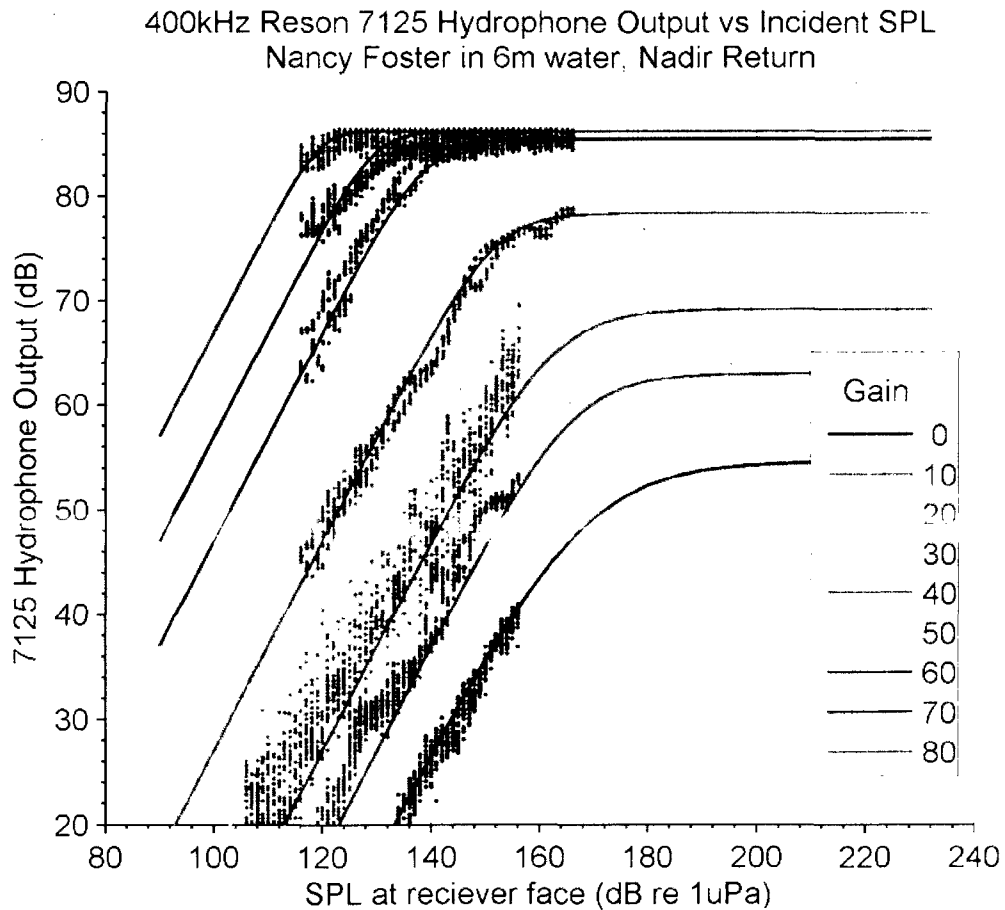


**Figure 22: Launch 2807 data over plotted on tank derived model. Beam formed data has been shifted -5 dB vertically and -67 dB horizontally.**

The *Nancy Foster* data were acquired in two parts while the vessel was at her home berth in Charleston NC. The data with gain settings above 30 dB were acquired five hours after the data with lower gains. No data at a gain setting of



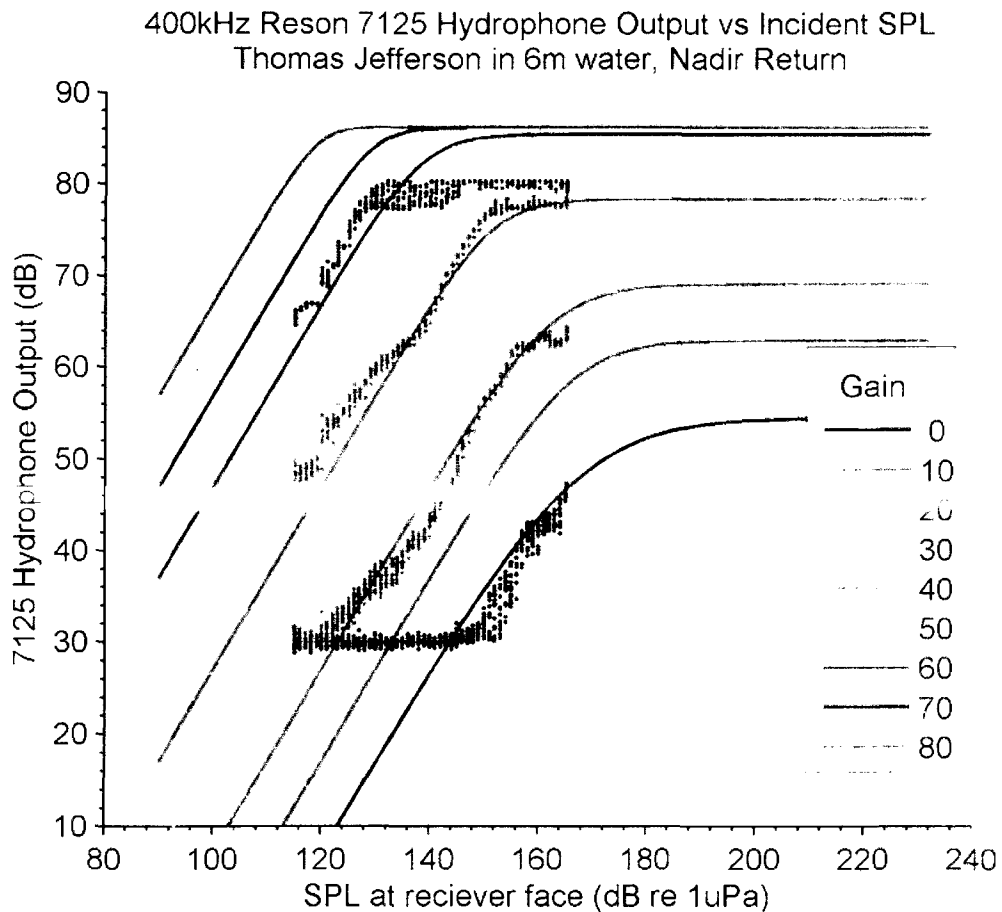
30 dB were acquired. Because the two data sets were acquired with the same instrument, the same vertical offset, -7 dB, has been applied to both sets of data on the assumption that the beam forming gain and sensitivity of the system is constant over that interval. Because the data sets were acquired at different locations on the pier and at different times in the tidal cycle, and so different heights above the sea bottom, different horizontal offsets were applied to appropriately match the data to the model. This accommodates the likely different target strength and transmission loss between the two tests.



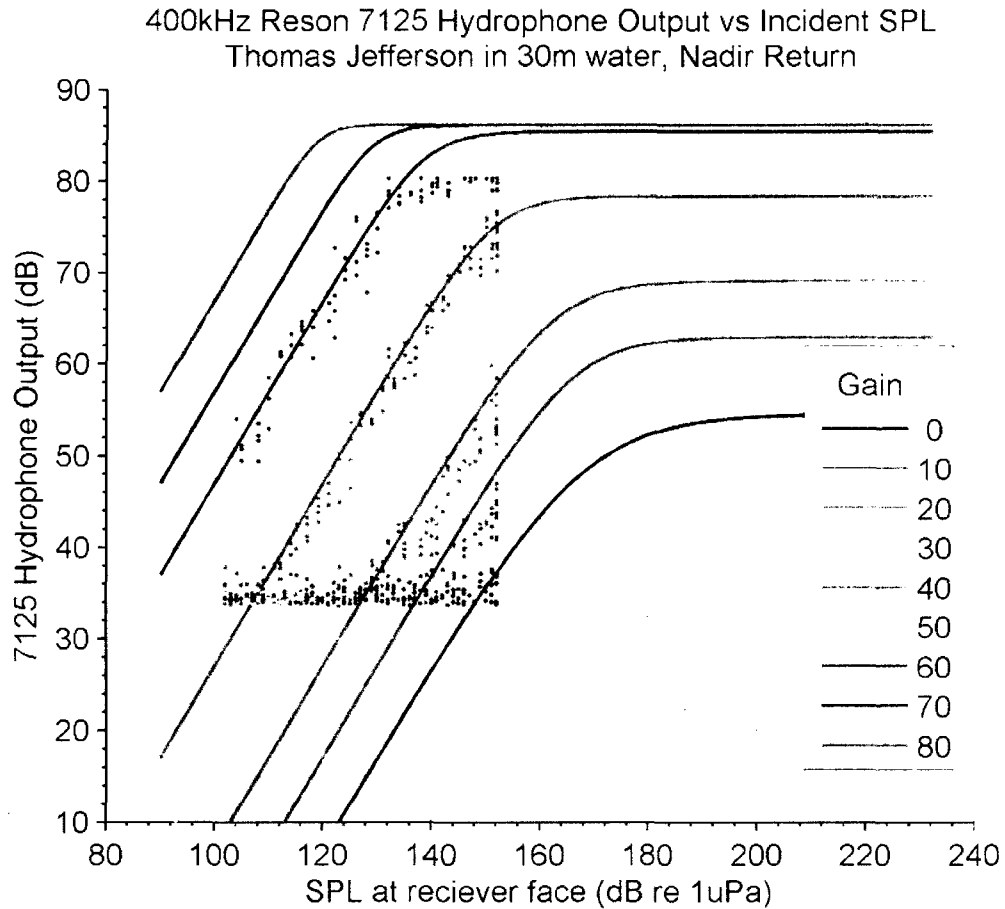
**Figure 23: Nancy Foster data over plotted on tank derived model. Data has been shifted -7 dB vertically and -54 dB horizontally for gains less than 40 dB, and -64 dB for remainder.**

Figure 24 shows the data acquired on the Thomas Jefferson while alongside her pier in Norfolk, VA. The seafloor at the pier is mud and the water depth was approximately 6 m below the transducer. No data were acquired at a gain setting of 10 dB. A vertical offset of -7dB and a horizontal offset of -55 dB has been applied to this data set.

Figure 25 shows data acquired by the same system on the Thomas Jefferson in 30 m of water over a sand bottom. These data were acquired while the ship was stopped for a oceanographic cast. The vertical offset is -7dB and the horizontal offset is -68 dB.



**Figure 24: Thomas Jefferson data from pier side tests over plotted on tank derived model. Beam formed data has been shifted -7 dB vertically and -55 dB horizontally.**



**Figure 25: Thomas Jefferson data from underway tests over plotted on tank derived model. Beam formed data has been shifted -7 dB vertically and -68 dB horizontally.**

**Field Acquisition Discussion**

All tests show the high gain-level nonlinearity, presumable clipping, that was observed in the test tank results. The tests in shallower water also show the high SPL level non-linearity. This is not seen in the deeper water test from Thomas Jefferson in 30m of water, likely because the returned SPL is too low.

The results from the tests over a mud bottom, e.g. Figure 24, show variations from linear behavior that does not appear to be related to the saturation phenomena observed in the tank. This is most likely due to variability in the target strength of the sea floor during the duration of the tests. Figure 26

shows a section of the water column data from the *Nancy Foster* test. A trail of what appears to be bubbles is seen rising from the mud. The presence of bubbles moving in and out of the selected target area makes the target strength highly variable because the target strength of a gas bubble is so different than the target strength of the displaced water or mud. The data from the *Thomas Jefferson* that were acquired at her home pier, also with a mud bottom, also shows significant apparent variations in target strength. Because this variation in target strength during the course of the experiment partially masks the linearity of the system response, these bottom types cannot be assumed to have constant target strengths, and are likely not as suitable for such tests as a bottom type with a more consistent target strength.

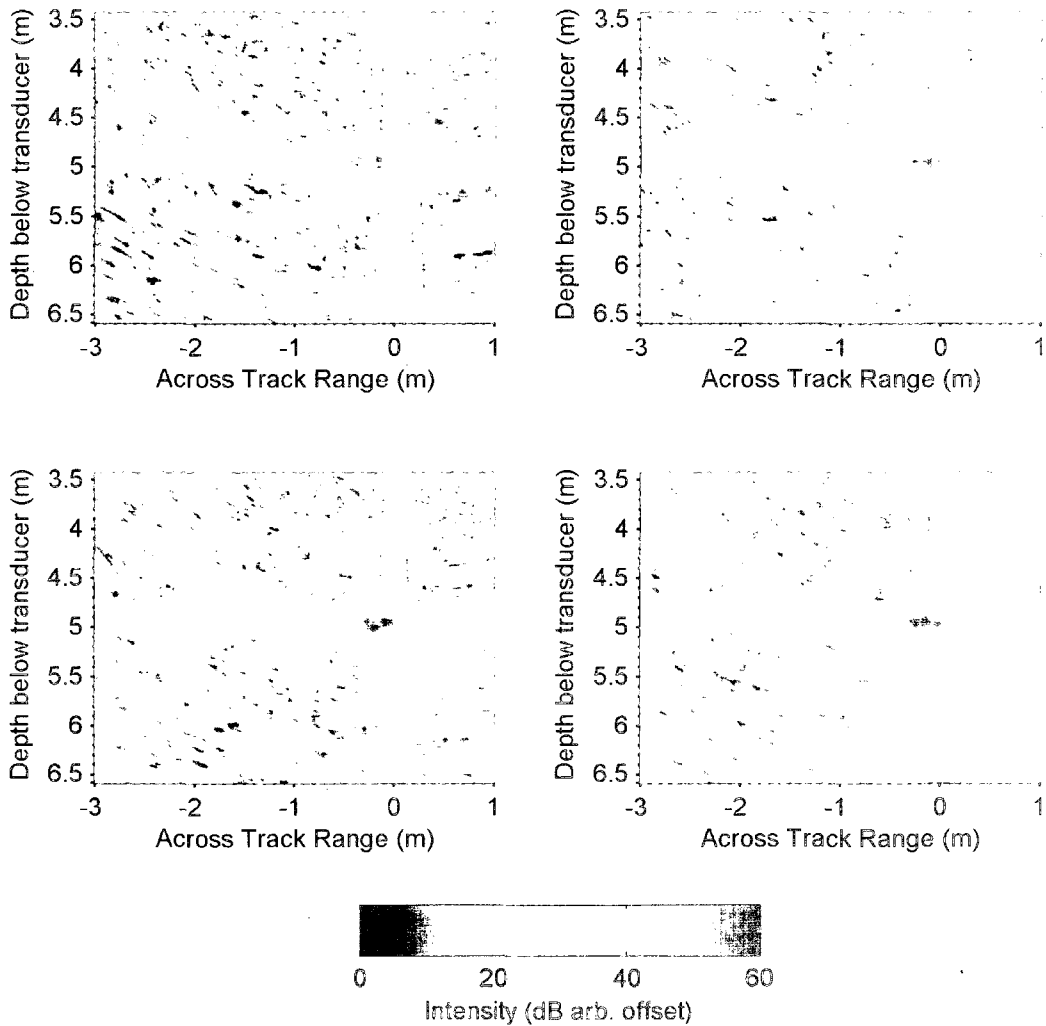


Figure 26: Segment of Nancy Foster test data showing apparent bubbles rising from mud bottom. Images are intensities of acoustic returns. Interval between images is 0.5 seconds.

The tests conducted on the *Thomas Jefferson* over a sandy bottom in approximately 30 meters of water demonstrate that such a test is possible in deep water, but without driving the system conclusively non-linear, the ambiguity between the vertical and horizontal offsets are difficult to resolve.

If the Rapp model developed from the element level data is used to model the output from these systems, the fitting process yields the correction necessary

to define 1 dB compression points for these systems. The vertical offset applied to align the beam formed field acquired data with the hydrophone response model is a sum of both the beam former gain of the field unit and any sensitivity difference between the deployed system and the reference system. This offset can be used to similarly adjust the 1 dB compression points from units relative to the output of the hydrophones of the system tested in the tank to units output by the beam former of the field deployed units. These are the data that is logged by these systems for backscatter purposes.

If the gain applied to the system is known, these corrected 1 dB compression points allow the data output to be evaluated for linearity. This evaluation can be done either in real time or with an archived data set.

## CHAPTER 3

### EFFECT OF NON-LINEARITY ON BACKSCATTER AND BATHYMETRY

In the previous chapters, the Rapp model for the gain-power linearity was introduced and was used to model the element level responses measured in a test tank. This model was also shown to describe the non-linear behavior of the beam formed response. Application of the APL\_UW backscatter model showed that non-linear behavior could be expected at high source levels for most bottom types in shallow water. Field tests carried out on sonar units mounted on operational platforms demonstrated that the corrections necessary to apply this model to those specific units could be determined in some cases. The field tests on operational units also directly show non-linear behavior in a realistic operational environment. In this chapter, the effect of non-linear behavior on both backscatter and bathymetry is evaluated.

The impact of signal clipping, which is a form of non-linearity, was discussed for hydrophone arrays by Anderson [35], Rudnick [36], and Remley [30]. The DIMUS (digital multibeam steering) system proposed by Anderson used polarity processing (very hard clipping), to digitally process output from a hydrophone array. The effect of amplitude and phase errors on arrays was addressed by Ramsdale and Howerton [37], Mucci and Pridham [38] and Quazi [39]. More recently, the effect of non-linear amplification on transmitted signals

has been an active area of interest in the satellite and wireless communications fields. In data communications, signals such as CW, FM, and FSK have constant amplitudes and are not particularly sensitive to non-linear effects. Signals that use both amplitude and phase modulation, however, are strongly impacted by nonlinear amplification. Examples of such signals in wide use for wireless telecommunications are QAM, OFDM, and QPSK [40]. In telecommunications, power efficiency of the transmitter, signal fidelity, and interference with adjacent channels are related to non-linear processes and are of significant concern.

For backscatter measurements with a MBES, non-linear effects on the amplitude can interfere with the interpretation of the data. Nonlinear processes may complicate efforts to normalize the data for image processing techniques. Nonlinearity may also change the measured statistics of the returned signal including the mean value. Because the nonlinear distortion depends on the amplitude of the incident signal, these changes may be modulated by the bottom topography and the backscatter coefficient of the bottom material.

Bathymetric measurements with a MBES are also impacted by nonlinear effects, largely through corruption of the beam forming process. Nonlinear processing of a narrow band signal introduces higher order harmonics. Depending on the system architecture, this distorted signal may not be beam formed correctly. Non-linear processes may be modeled as introducing amplitude and phase noise. Noise in the elements of an array has been shown to effectively both broaden the main lobe of the array response and increase the



sidelobe levels. This effect is demonstrated with data acquired in both the field and the tank.

For bathymetric measurements, increased sidelobe levels may lead to increased noise and poor bottom detection solutions. For bathymetric survey operations, targets proud of the bottom such as wrecks and boulders are of particular concern. These features can have much higher target strength than the surrounding seafloor, and in shallow water may drive the system into strongly nonlinear behavior for certain operating parameters. Successful bottom detection across the swath in these circumstances requires effective sidelobe suppression. We show that strong nonlinearity can cause markedly increased sidelobe levels in this situation, and show an example of poor data quality that may have been caused by this effect.

### **Effect of Non-Linearity on Backscatter**

Non linear performance of the MBES system may have a significant impact on the analysis of the backscatter data. One simple effect from non-linear system response has to do with the application of radiometric corrections. If the system response is non-linear then linear corrections to radiometric adjustment does not normalize the signal. If, for instance the receiver is saturated with respect to SPL, an increase in transmitted power does not increase the output signal from the system. If the output data are corrected to accommodate the increased transmit power, an artifact is introduced in the corrected data. More generally, if linear corrections do not normalize the data, then the system was behaving in a nonlinear fashion. This issue can be effectively avoided by

operating the system consistently and not changing any parameters, but this may not be an acceptable solution in many cases.

Other effects on backscatter processing may be more subtle and may depend on the processing technique used to analyze the backscatter data. In most cases for returns off a seafloor, the strength of the returned signal varies with angle. If the system response was non-linear, the distortion would be angularly dependent and confound analysis of the angular response of the seafloor. The stronger signals from closer to nadir are more distorted than the weaker signals from farther out on the swath. This tends to flatten the inner segment of the angular response curve.

As an example, Figure 27 shows the angularly dependent backscatter acquired over a relatively flat seafloor. These data were acquired by the *Thomas Jefferson* while travelling slowly, after an oceanographic cast. A time varied gain was applied to the system based on  $30\log R$  spreading loss and 110 dB/ km absorption loss. The power and transmitted pulse length of the system were fixed and the gain varied over the operating range. Subplot A shows the nadir response as a function of applied gain. At higher gain settings, the response is clearly nonlinear. Subplot B shows the angular dependent response of the output averaged over all pings in a test. These data were corrected for applied gain, i.e. for an applied gain of 10 dB, 10 dB has been subtracted from all data prior to plotting. This normalization is effective for low gain setting where the system response is linear, but not at higher gain values when the system response is nonlinear. Additional corrections would be required to extract a

better estimate of the true angular response of the seafloor, but for this case, those same corrections would need to be applied to across all the data, so the differences between this relatively crudely corrected angular backscatter would persist to a more appropriate treatment. Subplot C shows a mosaic image with sequential pings on the y-axis and beam number on the x axis. The intensity is mapped to a grayscale. The black bands are data gaps separating each of the tests. As with the angular response curves in subplot B, the data has been corrected for applied gain.

At a gain setting of approximately 40 dB, the nadir response begins to show substantial compression. This modifies the angular response curve at angles close to nadir. At higher gain settings, the system saturates across the swath and all angular response information from the seafloor is obliterated.

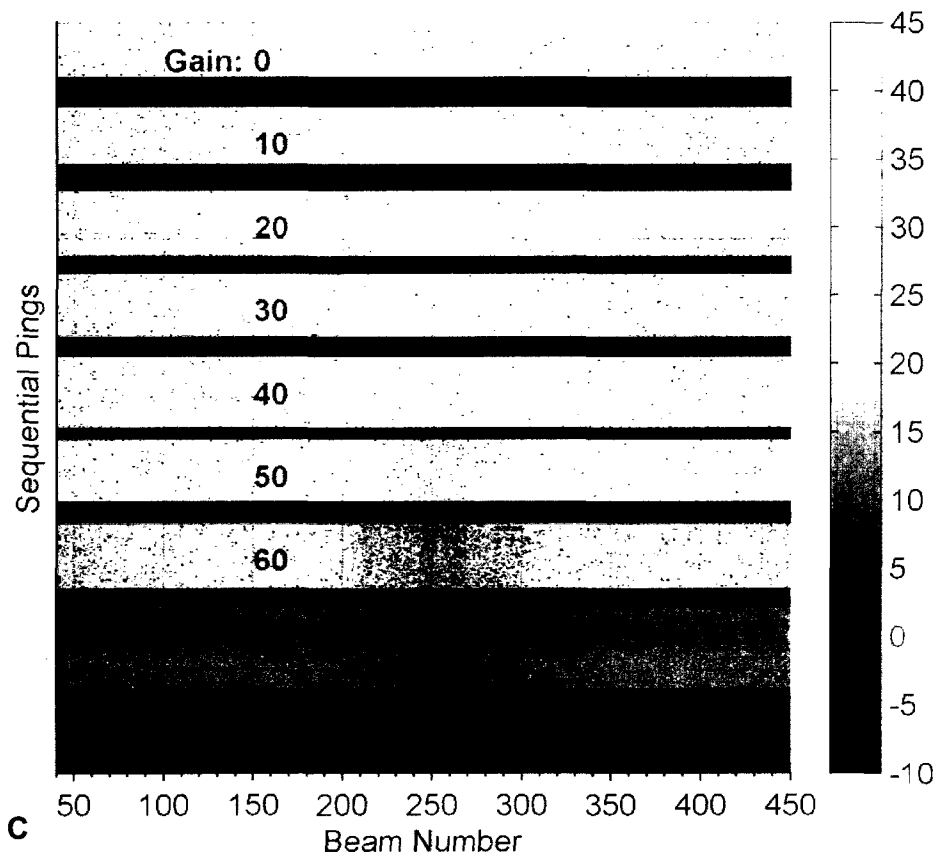
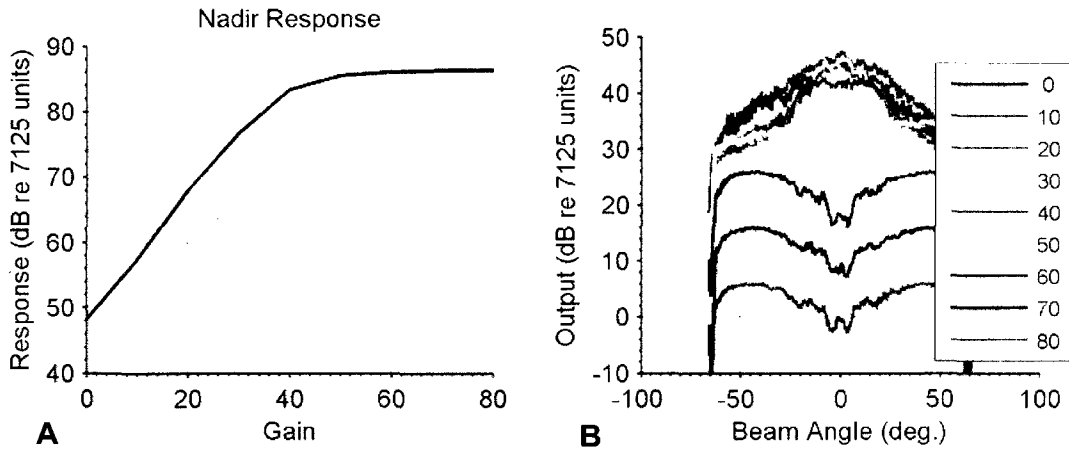


**Figure 27: Impact of non-linearity on backscatter. A.** Output of nadir beam with increasing gain. Output signal begins to saturate at approximately 40 db of gain. **B.** Average angular response for each gain setting. **C.** Image of backscatter across swath for sequential pings. Black bands are gaps in data. Patches of different material are visible in sections with gain of 0 and 20.

If the statistics of the distribution of backscatter returns are used to interpret the data, the distributions will be skewed by a nonlinear process. The dynamic range of the distribution will be reduced by gain compression and the upper tail of the distribution will be truncated. Using the same data set described in the previous example, the effect of nonlinearity on distributions is shown in Figure 28. Histograms of the backscatter from  $40^\circ$  to  $50^\circ$  are shown for four different gain settings. Distortion of the shape of the distribution is apparent as well as a shift in the mean.

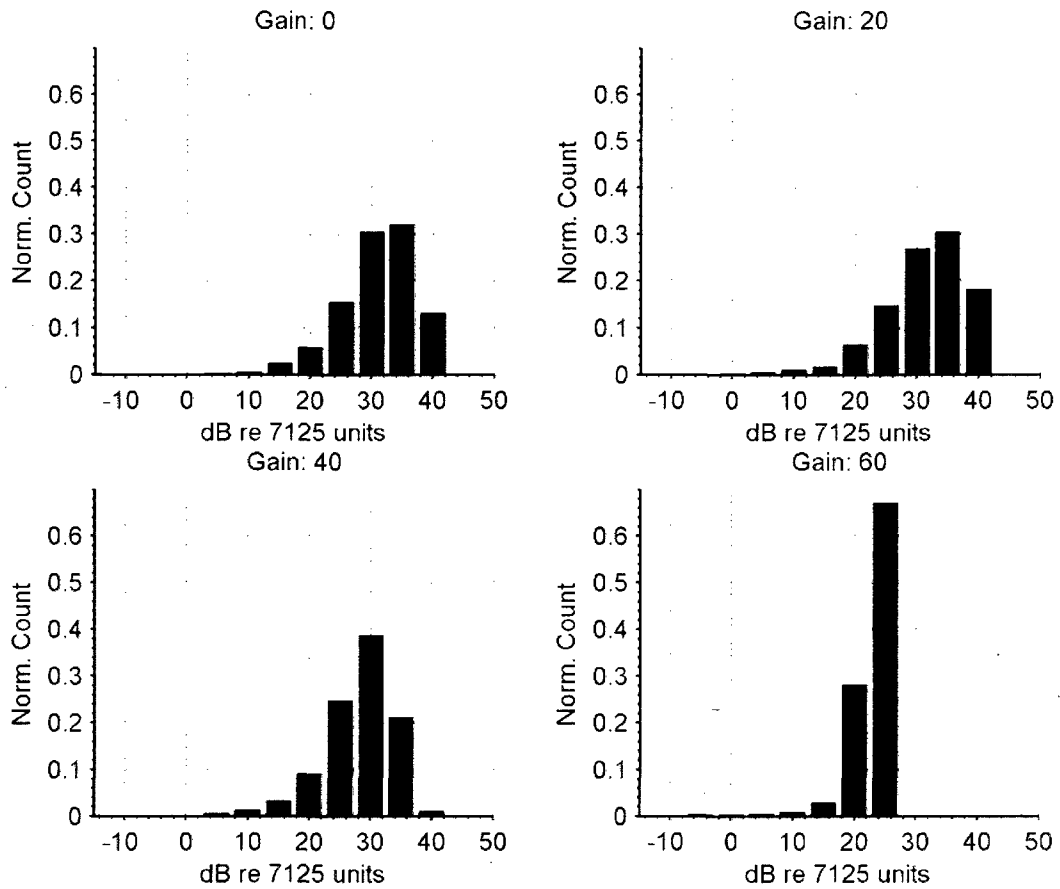


**Figure 28: Histograms of backscatter from 40° to 50° at increasing gain. The shape of the distribution is distorted at high gain settings.**

### **Effect of Non-Linearity on Beam Forming and Bathymetric Detection**

Non-linear processes may also have an impact on the beam forming process. In some cases these effects may also have an impact on the acquisition of bathymetric depth data. The effect of non-linearity on beam-forming is evaluated from two perspectives. The first considers the effect of a nonlinear processing step prior to beam forming. The second approach models nonlinear distortion as amplitude and phase noise on the individual elements.

First consider a pure sine wave signal input into a non-linear device and then fed through a beam forming process. The incident signal has spectral content at only one frequency,  $f_0$ . The wave form and spectral content of this signal are shown in Figure 29. Following the non-linear process, the output signal will have the fundamental frequency plus higher order harmonics. In the limit of very high distortion, the output waveform will approach a square wave. Using a Fourier series expansion, a square wave can be written as

$$f(t) = \frac{4}{\pi} \sum_{n=1,3,5,\dots} \frac{1}{n} \sin(2\pi n f_0 t) \quad (21)$$

This frequency content at the harmonic frequencies of a square wave is shown in Figure 30. The amplitude of the square wave has been set so the total power is the same as the sine wave shown in Figure 29.

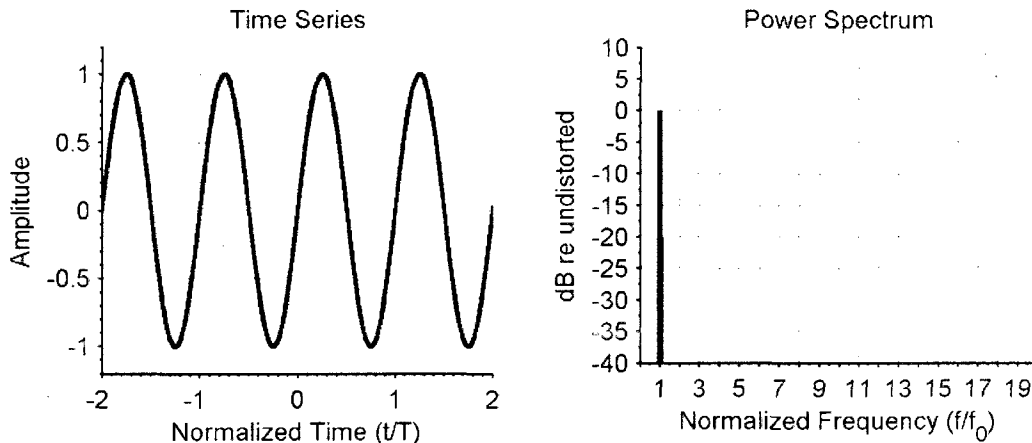


**Figure 29: Time series and frequency content of undistorted sine wave**

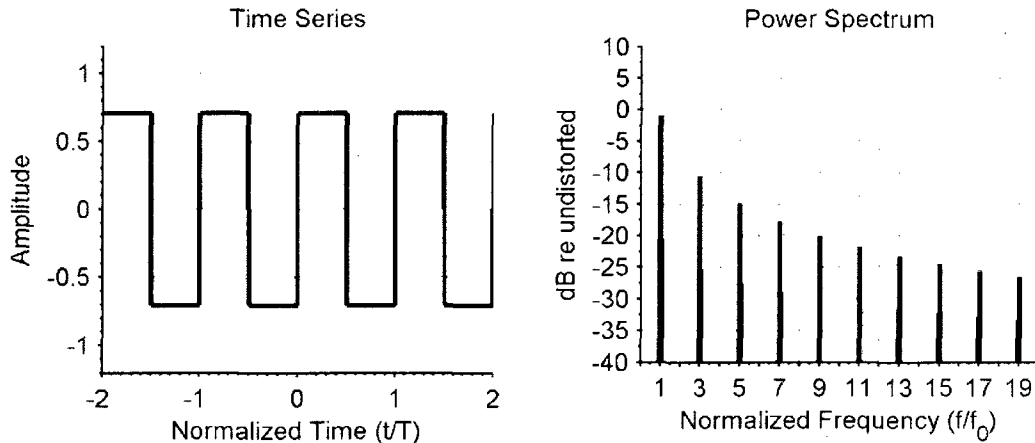


**Figure 30: Time series and frequency content of square wave. A square wave can be seen as the limiting case for a distorted sine wave.**

If filters are included in the receiver architecture after the non-linear process, these higher order harmonics could be effectively removed and have little to no impact on the beam forming process. If these harmonics are not completely removed before the beam forming step, they may interfere with the beam forming output through creation of lobes at angles away from the desired axis.

Recognizing again that the beam forming process is linear with respect to the element level response, the fundamental and harmonic components can be analyzed separately

In order to avoid grating lobes in a steered linear array, elements are typically placed at a maximum separation distance of one half the wavelength of the incident wavelength [26] or

$$d \leq \frac{\lambda}{2} \tag{22}$$

In general, an array suffers from grating lobes when the path difference is an integer number

$$\sin \Theta_n = n \frac{\lambda}{d} \quad n = 1, 2, 3, \dots \tag{23}$$



This equation clearly has no solution for  $d=\lambda/2$ , but for the higher order harmonics it may. The wavelength of the harmonics are smaller than the fundamental and are given by

$$\lambda_n = \frac{\lambda_0}{n} \quad n = 3,5,7, \dots \quad (24)$$

where  $\lambda_0$  is the fundamental wavelength and  $\lambda_n$  are the wavelengths of the harmonics. If the elements are assumed to be spaced at  $d=\lambda_0/2$ , the angles of the grating lobes for the first three harmonics are given by:

$$\text{1st harmonic:} \quad \theta_n = 42^\circ \quad (25)$$

$$\text{2nd harmonic:} \quad \theta_n = 23^\circ, 53^\circ \quad (26)$$

$$\text{3rd harmonic:} \quad \theta_n = 17^\circ, 35^\circ, 59^\circ \quad (27)$$

These angles would be different if the element spacing were not at exactly  $\lambda/2$ . Unlike grating lobes formed by an under-sampled array, the magnitude of the grating lobes would be significantly reduced from the main lobe because of the  $1/n$  factor in the amplitude of the harmonic. For a square wave input with no filtering, the grating lobes from the 1<sup>st</sup> harmonic would be approximately 10 dB down from the main lobe.

The interaction of a non-linear process with the receiving sonar architecture is likely to be significantly more complex than was modeled in the simple cases above. In addition to the harmonic frequencies discussed above, there may also be intermodulation products between the various harmonics and the local oscillator, amplitude modulation to phase modulation conversions, direct feed through of the mixer, and other effects [27]. Without knowledge of or access to the circuitry of the receiver, prediction and modeling of these effects is difficult.

Lacking a good model for these effects, they can be modeled as random amplitude and phase noise. Ramsdale and Howerton [37] showed that random errors in amplitude and phase of the elements of a linear array introduce a background sidelobe level that cannot be effectively reduced through the use of shading methods.

The effects of nonlinear processing on sidelobe levels was investigated for an operational MBES by taking the sample across all beams corresponding to the time of the nadir bottom detection. This essentially generates the nadir-pointing sidelobe level across all beams. As with the backscatter data discussed in the previous section, these data were acquired by the *Thomas Jefferson* while travelling slowly, after an oceanographic cast. A time varied gain was applied to the system based on  $30\log R$  spreading loss and 110 dB/ km absorption loss. The power and transmitted pulse length of the system was fixed and the gain varied over the operating range. Figure 31 shows nonlinearity in the system response effectively increases the sidelobe levels and broadens the shoulders of the main beam at nadir. While this is not, strictly speaking, a beam pattern measurement, it is a measurement of the effect of sidelobes on a real seafloor.

Figure 32 shows an example of problems with bathymetric bottom detection solutions caused by sidelobes. This data set was acquired during a production survey by a Reson 7125 in approximately five meters of water over a patch of rock outcrops, transmit power was at full and the nadir return is likely fully saturated. Sidelobe detections are circular arcs touching the seafloor at nadir.

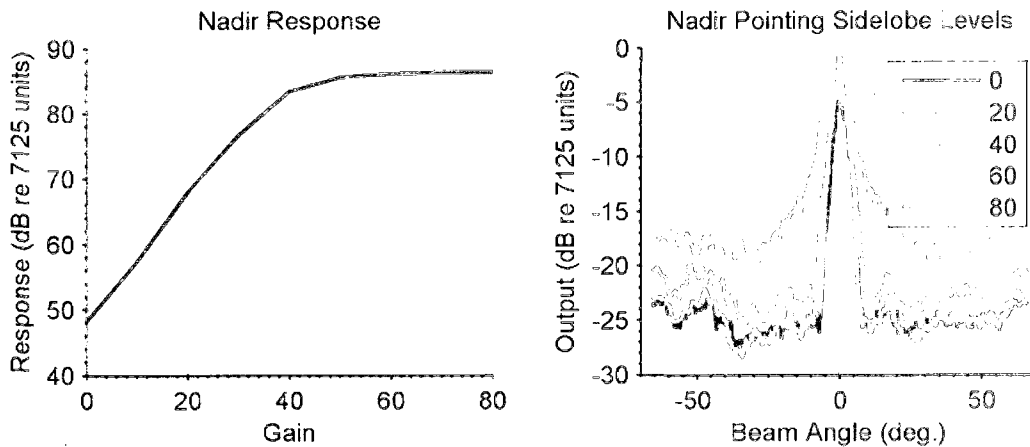


**Figure 31: The effect of nonlinear process on sidelobe levels.**

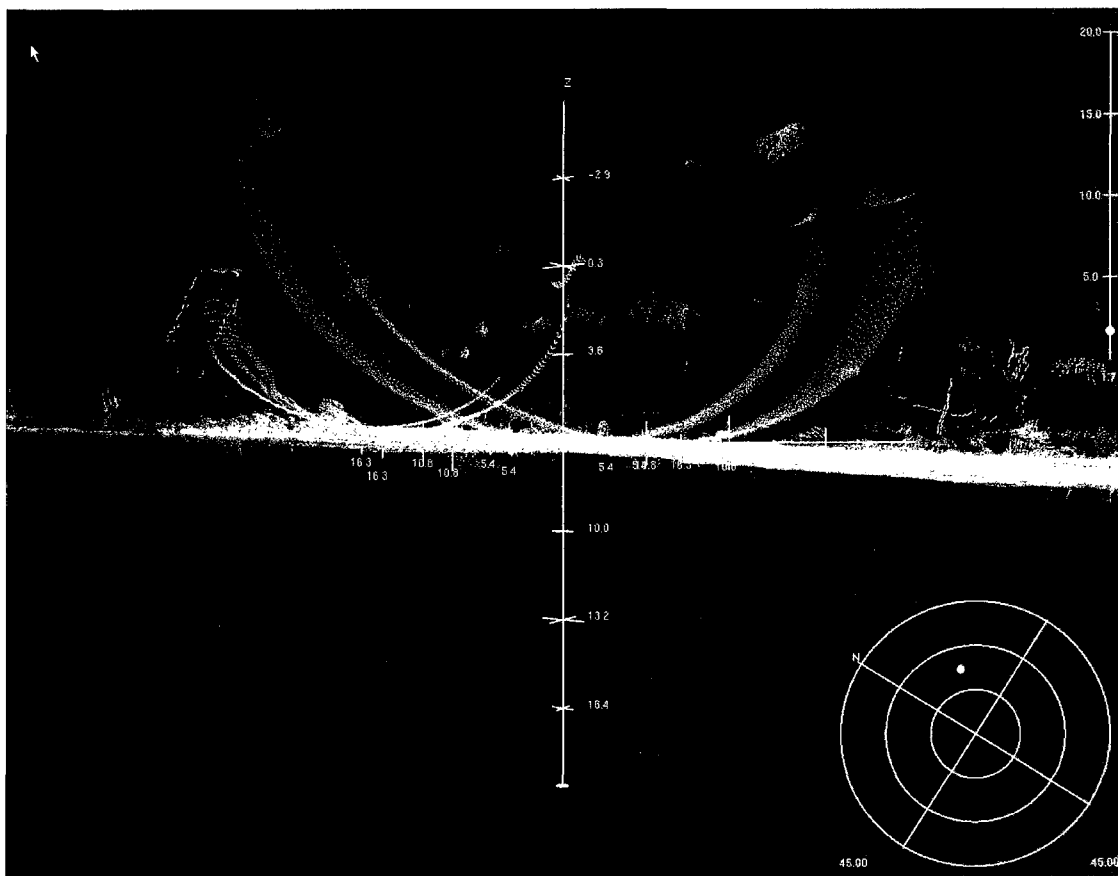


**Figure 32: Sidelobe detections. Individual detection of a MBES system are shown by dots, colored by swath. Gray dots have been manually flagged as noise. These are detections on sidelobes. System was operated at full power in 5 m depth.**

## CHAPTER 4

### CONCLUSION

The backscatter information available from many modern MBES systems has been shown to be useful for a number of purposes. These data are increasingly acquired both as an ancillary product to bathymetric surveys and as a primary data product from MBES surveys. To date, methods for calibrating and characterizing the amplitude response of MBES systems lag far behind those developed for fisheries applications using single or split beam systems. Until full calibrations of installed MBES systems are feasible, it may be sufficient for many purposes to characterize some aspects of the sonar performance. Linearity of the system response is a critical aspect of analytical use of this data. We have developed methods for measuring the linearity of a MBES system in both a test tank environment and in the field. A two-parameter nonlinear model developed for high power amplifiers was used to successfully model the nonlinear behavior of this system. This model provides a framework for understanding the results obtained from operational units installed on survey vessels. The Reson 7125 can be driven into a nonlinear behavior in shallow water when operated at high power or gain settings.

Nonlinear behavior was shown to have an adverse impact on backscatter processing methods by complicating radiometric corrections, corrupting the measured angular response of the seafloor, and distorting the statistics of the backscatter. In addition, nonlinear system behavior has also been demonstrated to adversely impact bathymetric data acquisition by corrupting the beam forming process. This was shown to lead to higher sidelobe levels and is posited to explain the sidelobe detections commonly seen with this system when operated at high powers over strong targets in shallow water.

Concerns over linearity of fisheries systems were settled by the introduction of systems with very high dynamic range in the late 1980's. Until such systems become widely available in MBES systems, the linear operating regimes of these systems should be characterized as part of their analytic use and operation outside the linear range should be avoided. Because nonlinear system response has an adverse impact on both backscatter and bathymetric processing, such restriction should not be viewed as a compromise of one data objective for the other.

## REFERENCES

- [1] V.E. Kostylev, R.C. Courtney, G. Robert, and B.J. Todd, "Stock evaluation of giant scallop (*Placopecten magellanicus*) using high resolution acoustics for seabed mapping," *Fisheries Research*, vol. 60, pp. 479-492, Feb. 2003.
- [2] J.A. Goeff, B.J. Kraft, L.A. Mayer, S.G. Schock, C.K. Sommerfield, H.C. Olson, S.P.S. Gulick, and S. Nordfjord, "Seabed characterization on the New Jersey middle and outer shelf: correlatability and spatial variability of seafloor sediment properties," *Mar. Geology*, vol. 209, pp. 147-172, Aug. 2004.
- [3] T.F. Sutherland, J. Galloway, R. Loschiavo, C.D. Levings, and R. Hare, "Calibration techniques and sampling resolution requirements for groundtruthing multibeam acoustic backscatter (EM3000) and QTC VIEW™ classification technology," *Estuarine Coastal and Shelf Science*, vol. 75, pp. 447-458, Dec. 2007.
- [4] C.J. Brown and P.B. Blondel, "Developments in the application of multibeam sonar backscatter for seafloor habitat mapping," *Appl. Acoustics*, vol. 70, pp. 1242-1247, Oct. 2009.
- [5] T.P. Le Bas and V.A.I. Huvenne, "Acquisition and processing of backscatter data for habitat mapping – Comparison of multibeam and sidescan systems," *Appl. Acoustics*, vol. 70, pp. 1242-1247, Oct. 2009.
- [6] A.J. Kenny, I. Cato, M. Desprez, G. Fader, R.T.E. Schüttenhelm, and J. Side, "An overview of seabed-mapping technologies in the context of marine habitat classification," *ICES J. of Marine Sci.*, vol. 60, pp. 411-418, Apr. 2003.
- [7] C. de Moustier and H. Matsumoto, "Seafloor acoustic remote sensing with multibeam echo-sounders and bathymetric sidescan sonar systems," *Mar. Geophys. Res.*, vol. 15, pp. 27-42, no. 1, pp. 27-42, Aug. 1993.
- [8] N.A. Cochrane, Y. Li, G.D. Melvin, "Quantification of a multibeam sonar for fisheries assessment applications," *J. Acoust. Soc. Amer.*, vol. 114, no. 2, pp. 745-758, Aug. 2003.
- [9] K.G. Foote, D. Chu, T.R. Hammar, K.C. Baldwin, L.A. Mayer, L.C. Hufnagle, Jr., J.M. Jech, "Protocols for calibrating a multibeam sonar," *J. Acoust. Soc. Amer.*, vol. 117, no. 4, pp. 2013-2027, Apr. 2005.
- [10] C. Lanzoni, S. Greenaway, T. Weber, "Reson SeaBat 7125 multibeam echo sounder calibration," Center for Ocean and Coastal Mapping/ Joint Hydrographic Center, University of New Hampshire, Durham, NH, 2009.
- [11] L. Fonseca and L. Mayer, "Remote estimation of surficial seafloor properties through the application Angular Range Analysis to multibeam sonar data," *Mar. Geophys. Res.*, vol. 28, no. 2, pp. 119-126, Jun. 2007.

- [12] V.E. Kostylev, B.J. Todd, G.B.J. Fader, R.C. Courtney, G.D.M Cameron, R.A. Pickrill, "Benthic habitat mapping on the Scotian Shelf based on multibeam bathymetry, surficial geology and sea floor photographs," *Mar. Ecology Progress Series*, vol. 219, pp. 121-137, Sept. 2001.
- [13] C. de Moustier, "Beyond bathymetry: mapping acoustic backscattering from the deep seafloor with Sea Beam," *J. Acoust. Soc. Amer.*, vol. 79, no. 2, pp. 316-331, Feb. 1986.
- [14] J. Hughes Clarke, "Towards remote seafloor classification using the angular response of acoustic backscattering: a case study from multiple overlapping GLORIA data," *IEEE J. Oceanic Eng.*, vol. 19, no. 1, Jan. 1994.
- [15] L. Fonseca, C. Brown, B. Calder, L. Mayer, Y. Rzhanov, "Angular range analysis of acoustic themes from Stanton Banks Ireland: a link between visual interpretation and multibeam echosounder angular signatures," *Appl. Acoustics*, vol. 70, pp. 1298-1304, Oct. 2009.
- [16] L. Hellequin, J.M. Boucher, and X. Lurton, "Processing of high frequency multibeam echo sounder data for seafloor characterization," *IEEE J. Oceanic Eng.*, vol. 28, no. 1, Jan. 2003.
- [17] A.N. Gavrilov and I.M. Parnum, "Fluctuations of seafloor backscatter data from multibeam sonar systems," *IEEE J. Oceanic Eng.*, vol. 35, no. 2, Apr. 2010.
- [18] D.A. Abraham and A.P. Lyons, "Reverberation envelope statistics and their dependence on sonar bandwidth and scattering patch size," *IEEE J. Oceanic Eng.*, vol. 29, no. 1, Jan. 2004.
- [19] J.R. Preston and D.A. Abraham, "Non-Rayleigh reverberation characteristics near 400 Hz observed on the New Jersey shelf," *IEEE J. Oceanic Eng.*, vol. 29, no. 2, Apr. 2004.
- [20] O.A. Misund, "Underwater acoustics in marine fisheries and fisheries research," *Reviews in Fish Biology and Fisheries*, vol. 7, no. 1, pp. 1-34, Mar. 1997.
- [21] H.P. Knudsen, "Gauging the reliability of acoustic instruments for fisheries surveys," *Proc. MTS/ IEEE Oceans*, Boston, MA, pp. 213-219, Sep. 2006.
- [22] K.G. Foote, H.P. Knudsen, G. Vestnes, D.N. MacLennan, and E.J. Simmonds, "Calibration of acoustic instruments for fish density estimation: a practical guide," *Int. Council for the Exploration of the Sea*, Copenhagen, Denmark, Coop. Res. Rep. No. 144, Feb. 1987.
- [23] K.G. Foote, "Calibration Reflector," *ICES Conference and Meeting*, 1989/ B:4.
- [24] E. Mailard, private communication, Jan. 2010.
- [25] C. Lanzoni and T.C. Weber, "High-resolution calibration of a multibeam echo sounder," *Proc. IEEE Oceans 2010 Conf.*, Seattle, WA, Sep. 2010, in press.
- [26] X. Lurton, *An Introduction to Underwater Acoustics*, Chichester, UK: Praxis Pub., 2002.
- [27] J.S. Kenney, "Nonlinear microwave measurement and characterization," in *The RF and Microwave Handbook*, M. Golio, Ed. Boca Raton, FL: CRC Press, 2001, ch. 4, sec. 4, pp. 4-33-4-52.

- [28] C. Rapp, "Effects of HPA-nonlinearity on a 4-DPSK/ OFDM-signal for a digital sound broadcasting system," *Proc. 2nd European Conf. Satellite Communications*, Liège, Belgium, pp. 179-184, October 1991.
- [29] J. Vuolevi and T. Rahkonen, "Some circuit theory and terminology," in *Distortion in RF Power Amplifiers*, Boston, MA: Artech House, 2003, ch. 2, sec. 1.3, pp. 15-18.
- [30] W.R. Remley, "Some effects of clipping in array processing," *J. Acoust. Soc. Amer.*, vol. 39, no. 4, pp. 702-707, Apr. 1965.
- [31] J. Laskar, B. Matinpour, S. Chakraborty, Receiver system design," in *Modern Receiver Front-Ends*, Hoboken, NJ: John Wiley and Sons, 2004, ch. 2, sec. 2.1, pp. 15-16.
- [32] T.I. Laakso, V. Välimäki, M. Karjalainen, and U.K. Laine, "Splitting the unit delay: tools for fractional delay filter design," *IEEE Signal Processing Magazine*, Jan. 1996.
- [33] "APL-UW High-Frequency Ocean Environmental Acoustic Models Handbook," Appl. Physics Laboratory University of Washington, Seattle, WA, Tech. Rep. APL-UW TR 9407, Oct. 1994.
- [34] "SeaBat 7125 High-Resolution Multibeam Echosounder System Operator's Manual, version. 6.02", Reson, Inc., Goleta, CA, Feb. 2008.
- [35] V.C. Anderson, "Digital Array Phasing," *J. Acoust. Soc. Amer.*, vol. 32, no. 7, pp. 867-870, Jul. 1960.
- [36] P. Rudnick, "Small signal detection in the DIMUS array," *J. Acoust. Soc. Amer.*, vol. 32, no. 7, pp. 871-877, Apr. 1960.
- [37] D.J. Ramsdale and R.A. Howerton, "Effect of element failure and random errors in amplitude and phase on the sidelobe level attainable with a linear array," *J. Acoust. Soc. Amer.*, vol. 68, no. 3, pp. 901-906, Apr. 1980.
- [38] R.A. Mucci and R.G. Pridham, "Impact of beam steering errors on shifted sideband and phase shift beamforming techniques," *J. Acoust. Soc. Amer.*, vol. 69, no. 5, pp. 1360-1368, Apr. 1981.
- [39] A.H. Quazi, "Array beam response in the presence of amplitude and phase fluctuations," *J. Acoust. Soc. Amer.*, vol. 72, no. 1, pp. 171-180, Jul. 1982.
- [40] F.H. Raab, P. Asbeck, S. Cripps, P.B. Kenington, Z.B. Popović, N. Potheary, J.F. Sevic, N.O. Sokal, "Power amplifiers and transmitters for RF and microwave," *IEEE Trans. Microw. Theory Tech.*, vol. 50, no. 3, Mar. 2002.